# E. WOLF, PROGRESS IN OPTICS XXIX © ELSEVIER SCIENCE PUBLISHERS B.V., 1991

I

## OPTICAL WAVEGUIDE DIFFRACTION GRATINGS: COUPLING BETWEEN GUIDED MODES

BY

DENNIS G. HALL

The Institute of Optics University of Rochester Rochester, New York 14627, USA

## **CONTENTS**

|      |   | PAG | ЗE |
|------|---|-----|----|
| § 1. | INTRODUCTION                            |     | 3  |
| § 2. | USES FOR WAVEGUIDE GRATINGS             |     | 5  |
| 8 3. | MODES SUPPORTED BY PLANAR OPTICAL WAVE- |     |    |
| 3    | GUIDES                                  |     | 14 |
| § 4. | NONPLANAR OPTICAL WAVEGUIDES            |     | 29 |
| § 5. | COUPLING BETWEEN GUIDED WAVES           |     | 30 |
| § 6. | SUMMARY                                 |     | 59 |
| LIST | OF SYMBOLS                              |     | 60 |
| REF  | ERENCES                                 |     | 62 |

## § 1. Introduction

STEWART MILLER introduced the term "integrated optics" in 1969 to refer to the miniaturized optical systems he envisioned as important for the future of optical communications. Two subsequent decades of research and development in this area, along with major breakthroughs in the optical fiber and semiconductor laser arenas, have led to the demonstration of many integrated optical components, devices, and systems, and to the introduction of commercial products that make use of this technology. Furthermore, interest in integrated optics as a basic technology has broadened to include not only telecommunications, but also other applications such as optical sensors, information storage and processing, medical instrumentation, navigation, and computing, to name just a few. In addition, there is a renewed emphasis on the importance of making the technology of integrated optics compatible with that of integrated electronics. The currently widespread use of the term "integrated optoelectronics" is a reflection of the attitude that optics and electronics are complementary technologies.

The central idea behind the concept of an integrated optical system is the ability to process and manipulate light that is trapped within the confines of an optical waveguide. Here, the term "light" is used in a loose sense. The wavelengths ( $\lambda$ ) of interest in both integrated and fiber optics are, for the most part, in the near-infrared region of the spectrum, with wavelengths  $0.8 < \lambda < 2 \,\mu m$ , rather than in the visible region. Most, but not all, optical waveguide structures confine light by the mechanism of total internal reflection (TIR). Although there are many specific types of optical waveguides, the most important distinction to be drawn is based on dimensionality. A planar, or slab, optical waveguide consists of a layer of elevated refractive index bounded above and below by regions of lower refractive index. Such a structure provides confinement along only one transverse coordinate axis, as illustrated in fig. 1a for a step-index, planar optical waveguide. A geometrical optics construct that illustrates a ray trapped by TIR between two surfaces also appears in fig. 1a. Another type of optical waveguide provides confinement along two transverse coordinate axes (fig. 1b). The refractive index boundaries in fig. 1 are depicted as sharp, but this is not an essential feature of an optical waveguide. Both graded-index and step-index structures are in common use.

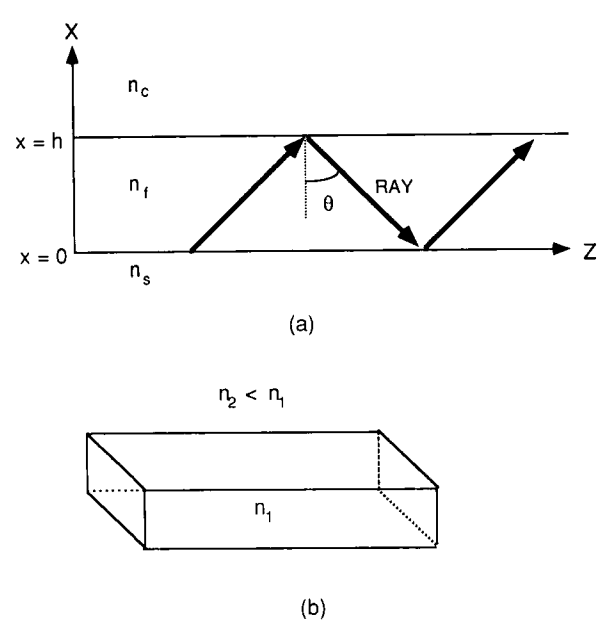


Fig. 1. (a) Planar, or slab, optical waveguide. The refractive index  $n_f$  of the film layer of thickness h must exceed that for each of the substrate  $(n_s)$  and cover  $(n_c)$  media. Refractive index barriers appear only along the x-direction. (b) Three-dimensional optical waveguide. The refractive index  $n_1$  within the guiding structure exceeds that outside the structure along both transverse directions.

This chapter focuses on one important structure for integrated optical/optoelectronic systems: the waveguide diffraction grating. Since the diffraction grating is a familiar component for conventional optical systems, it is logical to assume that it will be for integrated optical systems as well. This has been demonstrated by the use of waveguide gratings in integrated optics for input/output couplers, filters, lenses, Bragg reflectors, distributed reflectors in lasers, and as phase-matching elements for nonlinear interactions.

The fact that electromagnetic waves propagating within an optical waveguide exhibit spatial profiles that depend on the transverse coordinates complicates theoretical treatments of the interaction with waveguide diffraction gratings. Despite numerous theoretical investigations, one case has proved particularly troublesome: the Bragg reflection of a guided wave within a corrugated planar optical waveguide. The planar waveguide supports modes with either of two polarizations – transverse electric (TE) or transverse magnetic (TM). These are defined later in this chapter. A guided wave of either polarization incident on a waveguide grating generates a strong back-reflected guided wave if the Bragg

condition is satisfied at least approximately. Almost all theoretical treatments of this problem are in agreement when both the incident and Bragg-reflected waves are TE waves. This is not the case, however, for TM waves, for which theoretical treatments are in serious disagreement. Recent theoretical and experimental efforts appear to have resolved this issue satisfactorily. This chapter describes the essential features of the guided-wave Bragg reflection problem that are crucial for a proper treatment of the problem. Sufficient preliminary material on the properties of optical waveguide modes in several structures is included to introduce the reader unfamiliar with the subject to the more important features common to all optical waveguides. Since a full discussion of both the theoretical controversy and its resolution has not yet appeared, sufficient theoretical detail has been included, particularly in the later sections, to allow others to carry out the various calculations. Hence, the introductory material is essential to make this chapter self-contained.

A qualitative review of the uses of the waveguide gratings mentioned earlier is followed by a more quantitative review of the properties of optical waveguides, with emphasis on the step-index planar waveguide. The step-index planar waveguide lends itself to relatively straightforward analysis while revealing the essential qualitative features that are common to all optical waveguides. Finally, the interactions between guided waves and waveguide gratings are considered from several theoretical points of view.

## § 2. Uses for Waveguide Gratings

#### 2.1. GENERAL DISCUSSION

Waveguide diffraction gratings can be fabricated as a periodic or near-periodic modulation of either the refractive index or one, or more, of the boundaries of an optical waveguide as illustrated in fig. 2. The surface corrugation grating is the more common, since it can be implemented in almost any solid material. Such surface gratings are usually prepared by recording the interference pattern, formed when the two halves of a laser beam recombine at a selected angle, in a layer of photoresist deposited onto the substrate of interest. After the photoresist has been developed, it serves as a mask for substrate etching by techniques such as ion-milling or reactive ion etching. The photoresist mask protects certain areas of the substrate while the etchant attacks the exposed areas. In this way the mask pattern is transferred into the substrate material.

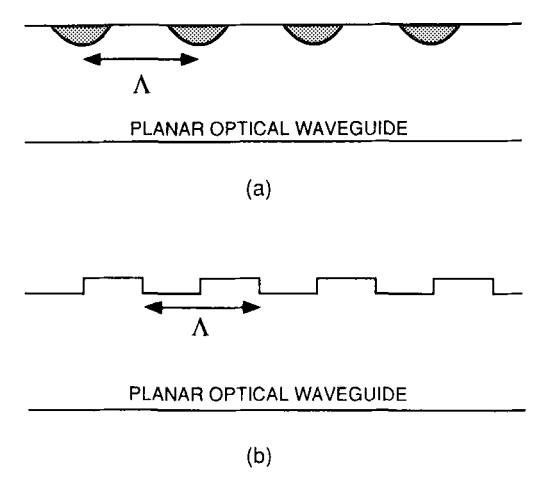


Fig. 2. Two types of waveguide diffraction gratings with period  $\Lambda$ . (a) A periodic variation of the refractive index near the surface. (b) A periodic surface corrugation.

A similar procedure can be used based on electron-beam lithography rather than photolithography.

There are two main uses for waveguide gratings in integrated optics. The first use, illustrated in fig. 3a, involves coupling between the radiation field and a bound mode of the optical waveguide. As the bound modes use total internal reflection, there is no exterior angle of incidence for which an external beam of light can be made to excite a bound mode of a waveguide with flat surfaces by refraction. Similarly, it is not possible for a guided mode to radiate in the absence of some coupling mechanism. The grating provides the necessary coupling when the following condition is fulfilled:

$$\beta = n_c \left(\frac{\omega}{c}\right) \sin \theta + \frac{2\pi m}{\Lambda},$$

where  $\beta$  is the propagation constant (along z) of the guided wave,  $\Lambda$  is the grating period, m is an integer,  $\omega$  is the (angular) frequency of the optical wave, c is the speed of light in vacuum, and the angle  $\theta$  and the refractive index  $n_c$  are identified in the figure. This type of interaction is clearly useful for coupling light into or out of an optical waveguide.

The second use, illustrated in fig. 3b involves coupling between two waves that are both bound modes of the optical waveguide. The grating can be used to deflect an incident guided mode into a different direction, or to convert a guided mode of one order into a guided wave of another order, or both. This

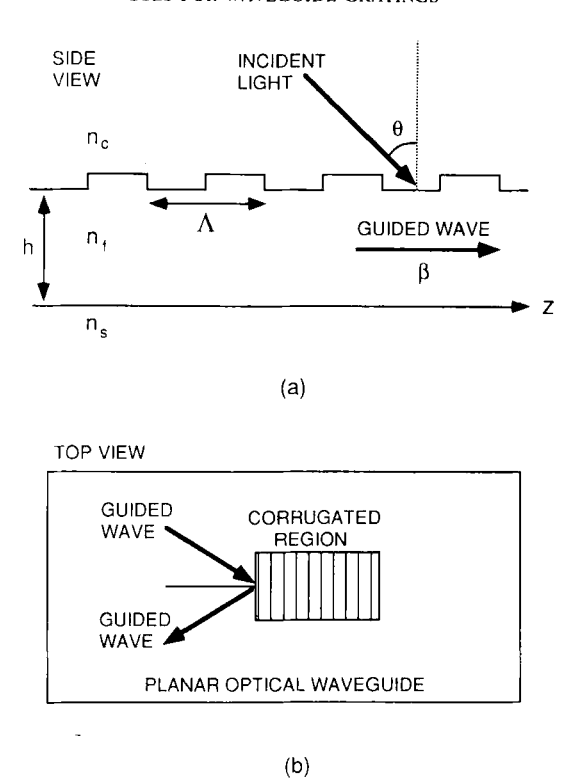


Fig. 3. (a) Light incident on a corrugated section of an optical waveguide can excite a guided mode of the structure. The grating acts as a phase-matching element to permit coupling between a guided mode and the radiation field. (b) A corrugated section of an optical waveguide can also provide coupling between two guided waves. In this example, a guided wave is Bragg reflected into a different direction within the waveguide.

type of interaction can be used for "in-plane" functions, examples of which appear in the following sections.

It is the period of the grating that determines which type of interaction takes place. A specific example will make this clearer. Consider the waveguide configuration in fig. 3a, but from the point of view of the guided wave interacting with the grating to produce another optical wave. If we define the *effective index* of refraction N according to

$$N=\frac{\beta}{2\pi\lambda}\,,$$

where  $\lambda$  is the optical wavelength (in vacuum), then it is not difficult to show that for guided wave propagation along z, the following first-order (m = 1)

phenomena occur for the indicated ranges of the ratio of the grating period to the wavelength,  $\Lambda/\lambda$ :

Radiation into the cover medium (x > h):  $(N + n_c)^{-1} \le \Lambda/\lambda \le (N - n_c)^{-1}$ . Radiation into the substrate medium (x < 0):  $(N + n_s)^{-1} \le \Lambda/\lambda \le (N - n_s)^{-1}$ . Back reflection (first-order):  $\Lambda/\lambda = (2N)^{-1}$ .

First-order back reflection (or Bragg reflection) occurs when a guided wave propagating along +z interacts with the grating to produce a guided wave of the same type propagating in the -z direction. Note that since  $n_s \le N \le n_f$  for  $n_s \ge n_c$ , a point that will be discussed later in this chapter, the smallest period in the preceding list is required for backreflection; radiation into either the substrate or cover media requires a period  $\Lambda/\lambda > (2N)^{-1}$ . There is some degree of overlap of the range of periods that produce radiation into the two media. For the usual case of  $n_s \ge n_c$ , this means that radiation into the cover medium is always accompanied by radiation into the substrate, but that a range of  $\lambda$  exists that produces radiation into only the substrate (refractive index  $n = n_s$ ).

## 2.2. INTERACTIONS BETWEEN GUIDED WAVES

An extensive literature exists that describes various demonstrations of the use of waveguide gratings. In one of the first such demonstrations, PENNINGTON and KUHN [1971] used gratings formed in a layer of photoresist deposited onto a planar, glass, optical waveguide to fabricate a multistage beam-splitter. After the photoresist was developed, lines of photoresist remained to serve as perturbations of the effective index of refraction of the glass waveguide. This is illustrated in fig. 4, which shows a guided wave, incident from the lower left, split into two beams, both still contained within the waveguide, by means of diffraction. This process is repeated for the other two gratings to produce a total of eight beams emerging from the grating on the right. A similar system was reported by Handa, Suhara, Nishihara and Koyama [1980] that used refractive-index gratings (fig. 2a), instead of surface gratings, made by direct electron-beam writing in arsenic trisulfide (As<sub>2</sub>S<sub>3</sub>) waveguides.

FLANDERS, KOGELNIK, SCHMIDT and SHANK [1974] demonstrated the spectral filtering property of a waveguide grating in the back-reflection geometry that appears in fig. 5. A surface corrugation grating was formed in the upper surface of a glass waveguide by first recording an interference pattern in a layer of photoresist deposited onto the glass layer. The pattern that remained

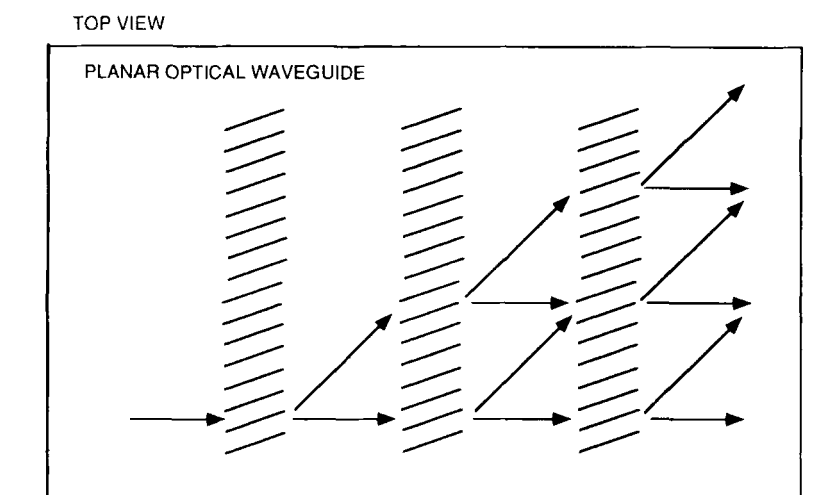


Fig. 4. Top view of a multistage beam-splitter fabricated in a planar optical waveguide.

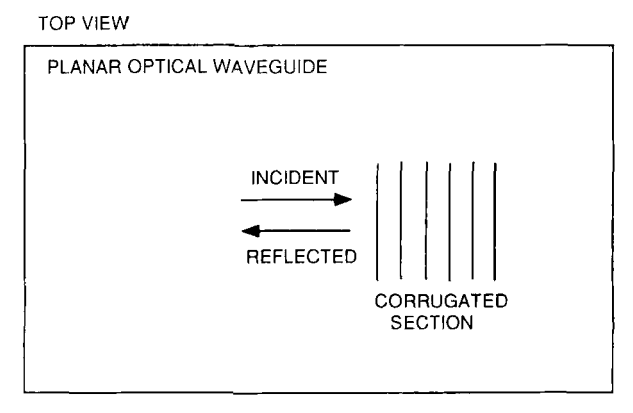


Fig. 5. Top view of the arrangement for a Bragg-reflection experiment using a planar optical waveguide.

after developing the photoresist was then transferred into the glass layer by means of ion-beam etching, resulting in an approximately 50 nm modulation in the thickness of the waveguide ( $\sim 0.85 \, \mu m$ ). A tunable dye laser was used to excite a guided wave propagating to the right (in fig. 5), which was subsequently back-reflected when the incident wavelength satisfied the Bragg condition. They reported reflectivities greater than 75% and reflection bandwidths less than 0.2 nm, thereby demonstrating that the grating can function as a

narrow-band reflector for use in integrated optics. The emphasis in their work was on narrow-band filters, although broad-band filters are also of interest (SHELLAN, HONG and YARIV [1977]).

Aperiodic gratings can also be useful for the coupling of two guided waves. LIVANOS, KATZIR, YARIV and HONG [1977] made use of a so-called "chirped" grating as a wavelength demultiplexer in the scheme illustrated in fig. 6. Here, the term "chirp" refers to the nearly linear variation in the grating period along the grating axis (z), which causes the wavelength that satisfies the Bragg condition to vary along z. When collinear guided waves excited by two independent sources with wavelengths  $\lambda_1$  and  $\lambda_2$  interact with the grating, the different wavelength components are diffracted at different locations along the grating. A glass waveguide was used in the experiment of Livanos and co-workers, along with a surface corrugation grating made by holographic exposure of photoresist followed by ion-beam etching, as discussed in the previous paragraph. The grating period varied between 0.293 <  $\Lambda$  < 0.321  $\mu$ m over a distance of 6.5 mm. This produced a separation of 4 mm between diffracted waves for  $\lambda_1 = 0.607 \ \mu$ m and  $\lambda_2 = 0.627 \ \mu$ m.

It is important, however, to note that waveguide gratings used at non-normal incidence (as in fig. 6) usually depolarize the incident wave. As will be discussed later in this chapter, a planar optical waveguide supports waves of two polarizations: transverse electric (TE) and transverse magnetic (TM). Fukuzawa and Nakamura [1979] demonstrated this effect by showing that an incident guided wave of the TE polarization produced both TE- and TM-diffracted waves. The TE- and TM-components are spatially separated, since the Bragg condition is slightly different for the two polarizations due to waveguide dispersion (the effective index of refraction N depends on the polarization, even

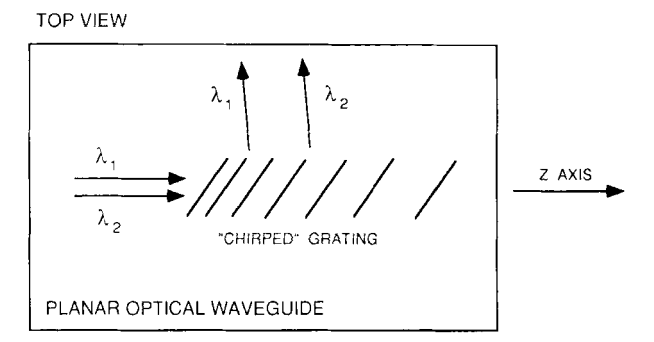


Fig. 6. Spatial separation of guided waves of two wavelengths using a "chirped" grating, for which the grating period varied along the length of the grating.

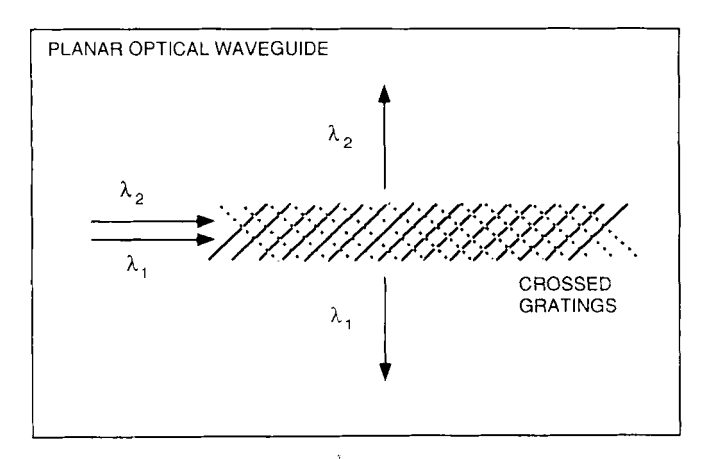


Fig. 7. Two crossed gratings fabricated in a planar optical waveguide. Incident guided waves with two different wavelengths are diffracted into opposite directions.

for a fixed wavelength). Therefore, although fig. 6 shows only two diffracted components, there will, in general, be four diffracted components, because of this polarization effect, a fact that could be important if a high degree of wavelength discrimination is required.

It is possible to use multiple exposure techniques to create a grating that diffracts guided waves of two wavelengths in opposite directions. The scheme used by YI-YAN, WILKINSON and LAYBOURN [1980], illustrated in fig. 7, makes use of crossed gratings, shown here as solid and dotted lines, on the surface of a glass optical waveguide to achieve the greatest possible spatial separation between the two wavelength components.

HATAKOSHI and TANAKA [1978] pointed out that a waveguide grating can function as a lens. They reported the use of a glass waveguide and a grating fabricated by electron-beam writing to focus a collimated input of wavelength  $\lambda = 488$  nm. Here, as shown in fig. 8, the orientation of the grating rulings is changed along the grating to make certain that each segment of the incident light is diffracted toward a common point.

One of the most important uses of waveguide gratings for the coupling of two guided waves occurs in the distributed feedback (DFB) and distributed Braggreflector (DBR) semiconductor lasers. The DFB laser was first discussed by Kogelnik and Shank [1971, 1972], and was first implemented in a semiconductor (waveguide) laser by Nakamura, Yariv, Yen, Somekh and Garvin [1973]. The ability of a waveguide grating to couple forward- and backwardgoing guided waves was discussed in connection with fig. 5. A strong reflection

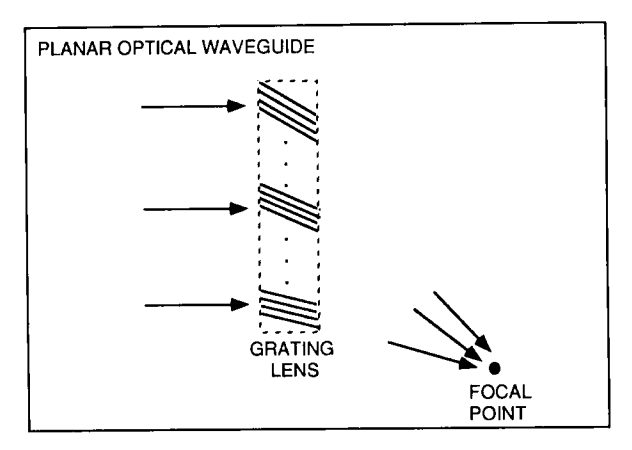


Fig. 8. A waveguide grating lens. The grating period and orientation can be adjusted continuously to deflect different portions of the incident wave toward a common point.

can be achieved within a narrow spectral bandwidth. The gain region of the laser is corrugated in a DFB laser so that the coupling between forward- and backward-going guided waves takes place throughout the laser cavity; hence, the term "distributed feedback". The DBR laser is somewhat similar to the DFB laser, except that only the unpumped end regions of the laser are corrugated in the DBR case; the gratings are used as passive reflectors. Both approaches take advantage of the narrow Bragg bandwidth of the corrugated waveguide to reduce the spectral width of the laser emission.

Waveguide gratings are also useful as phase-matching elements in nonlinear optics. This seems to have first suggested by SOMEKH and YARIV [1972]. In the case of second-harmonic generation, for example, it is necessary that the propagation constant of the wave at frequency  $2\omega$  (nearly) equal twice that of the wave at  $\omega$ . This cannot be easily achieved in all materials, but in a corrugated waveguide the grating constant provides an extra contribution to the phase-matching argument so that the matching condition becomes  $\beta(2\omega) = 2\beta(\omega) + 2\pi/\Lambda$ , in first order. The ability to vary both the grating period and the waveguide thickness within reasonable limits allows greater control over the phase-matching condition in a periodic waveguide than in a non-periodic medium.

The many uses that have been found for grating-induced coupling between guided waves makes it clear that a quantitative description of the strength of the coupling interaction is essential. This subject constitutes the main emphasis of this chapter.

## 2.3. INTERACTIONS BETWEEN GUIDED WAVES AND THE RADIATION FIELD

Waveguide gratings can be used for the excitation of a bound mode by an incident optical beam or to allow a bound waveguide mode to radiate. This point was discussed earlier in this section. Dakss, Kuhn, Heidrich and Scott [1970] appear to have been the first to use a grating to excite a guided wave. They used photolithographic techniques to form a photoresist grating with a period  $\Lambda=0.665~\mu m$  on the surface of a planar glass optical waveguide. Light from a helium-neon laser ( $\lambda=0.6328~\mu m$ ), incident as shown in fig. 3a, was used to excite either the TE or TM modes of the waveguide for the proper choice of source polarization. They reported an input coupling efficiency of 40%.

Input coupling efficiencies that exceed 40% are also possible. DALGOUTTE [1973] achieved an efficiency of 70% using a photoresist grating and a glass optical waveguide. One interesting feature of this experiment was the use of "reverse coupling", shown in fig. 9. In the actual experiment, light was incident on the lower surface of the waveguide through a prism (not shown) placed in contact with the substrate. Efficient coupling occurs when there is only one incident beam that can couple to the guided mode of interest. As pointed out earlier, there is a range of the grating period  $\Lambda$  for which a guided mode can radiate into the substrate, but not into the cover medium. The guided wave can be excited most efficiently when light is incident at this same unique angle of radiation. In Dalgoutte's experiment a grating period of 0.222  $\mu$ m was used to achieve this.

Many similar experimental results have been reported using different materials, different fabrication techniques, or different types of gratings. The use of blazed gratings has been explored by GRUSS, TAM and TAMIR [1980].

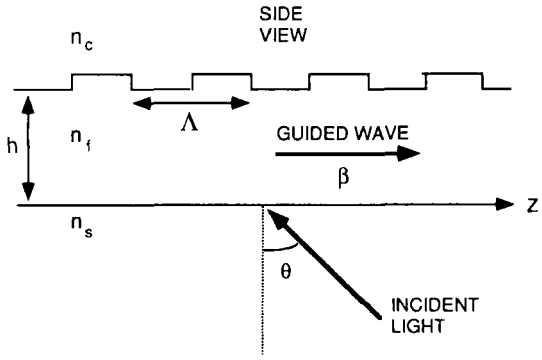


Fig. 9. Scheme for exciting a guided wave using the reverse-coupling technique.

The use of ion-implanted gratings has been demonstrated by KURMER and TANG [1983]. The importance of absorption losses on grating performance was considered by STONE and AUSTIN [1976]. Most recently, gratings have been used as output-couplers to make surface-emitting semiconductor lasers (EVANS, HAMMER, CARLSON, ELIA, JAMES and KIRK [1986], MACOMBER, MOTT, NOLL, GALLATIN, GRATRIX, O'DWYER and LAMBERT [1987]) and as focusing couplers for integrated read/write heads for optical data storage systems (SUHARA and NISHIHARA [1986]).

## § 3. Modes Supported by Planar Optical Waveguides

#### 3.1. BOUND MODES OF THE STEP-INDEX OPTICAL WAVEGUIDE

The planar, step-index, optical waveguide (fig. 1a) supports electromagnetic modes of two polarizations: transverse electric (TE) modes, and transverse magnetic (TM) modes. The term "mode", as it is used here, refers to a solution to the wave equation that satisfies the appropriate boundary conditions. Each such mode is an electromagnetic wave with a unique transverse field profile and propagation constant  $\beta$  (MARCUSE [1974], KOGELNIK [1975], ADAMS [1981], HALL [1987]). Optical waveguides are open structures that support both bound modes and radiation modes. For bound modes only certain discrete values of  $\beta$  are allowed. For radiation modes  $\beta$  is continuous within a certain prescribed range of values. This section considers the bound modes.

TE modes are characterized by a single electric field component that is oriented perpendicular to the direction of propagation. TE modes are thus specified by an electric field *E* of the form

$$E = \hat{\mathbf{y}} E_m(x) e^{i(\beta z - \omega t)}, \tag{1}$$

where the hat (^) designates a unit vector, in this case along the y-direction,  $E_m(x)$  is the TE mode function, m is an integer,  $\beta$  is the propagation constant with propagation assumed in the z-direction, and  $\omega$  is the (angular) frequency. TM modes are, in like manner, specified by a single transverse component of the magnetic field H according

$$H = \hat{\mathbf{y}} H_m(x) \,\mathrm{e}^{\mathrm{i}(\beta z - \omega t)} \,, \tag{2}$$

where  $H_m(x)$  is the TM mode function. Since  $\beta$  is discrete, it would be reasonable to attach the mode-integer subscript m, as in  $\beta_m$ , but we will suppress this subscript to  $\beta$  for the present to preserve simplicity of notation. When the above

fields are inserted into the usual wave equations for each medium,

$$\nabla^2 E + n^2 (\omega/c)^2 E = 0, \tag{3}$$

and

$$\nabla^2 \mathbf{H} + n^2 (\omega/c)^2 \mathbf{H} = 0 \,, \tag{4}$$

with n(x) defined in piecewise fashion,

$$n^{2}(x) = n_{c}^{2} \quad x > h$$
,  
 $= n_{f}^{2} \quad 0 < x < h$ ,  
 $= n_{s}^{2} \quad x < 0$ , (5)

we find that the TE mode function is given by

$$E_{m}(x) = E_{c} \exp \left[ -\gamma_{c}(x - h) \right] \quad x > h ,$$

$$= E_{f} \cos (k_{f}x - \phi_{s}) \qquad 0 < x < h ,$$

$$= E_{s} \exp \left( -\gamma_{s}x \right) \qquad x < 0 ,$$
(6)

where  $E_c$ ,  $E_f$ , and  $E_s$  are constants. The remaining parameters satisfy

$$y_i^2 = (\beta^2 - n_i^2 k_0^2)^{1/2} \quad (i = c, s), \tag{7}$$

$$k_f^2 = (n_f^2 k_0^2 - \beta^2)^{1/2}, \tag{8}$$

with  $k_0 = \omega/c = 2\pi/\lambda$ , and  $\phi_s$  is just the TIR phase-shift angle associated with the lower interface;  $\phi_s$  is defined by

$$\tan \phi_{i} = \frac{\gamma_{i}}{k_{f}} \quad (i = c, s), \qquad (9)$$

for the case of TE modes. The mode function for the TM modes has the similar form

$$H_{m}(x) = H_{c} \exp \left[ -\gamma_{c}(x - h) \right] \quad x > h ,$$

$$= H_{f} \cos \left( k_{f} x - \phi_{s}^{tm} \right) \quad 0 < x < h ,$$

$$= H_{s} \exp \left( -\gamma_{s} x \right) \quad x < 0 , \tag{10}$$

where  $H_c$ ,  $H_f$ , and  $H_s$  are constants, and the parameters are defined in the same way for TE and TM modes. The phase-shift angle for the TM polarization is slightly different from that in eq. (9),

$$\tan \phi_i^{\text{tm}} = \frac{n_f^2 \gamma_i}{n_i^2 k_f} \quad (i = c, s). \tag{11}$$

The requirement that the wave must be localized in or near the higher-index layer  $(n_f > n_s, n_c)$  determines that  $\beta$  is restricted to the range  $n_s k_0 \le \beta \le n_f k_0$ . It further requires that the mode functions  $E_m(x)$  and  $H_m(x)$  exhibit exponential decay with increasing distance from each interface. The application of the boundary conditions on the tangential components of E and E produces a dispersion relation given, for TE modes, by

$$k_{\rm f}h - \phi_{\rm c} - \phi_{\rm s} = m\pi \,. \tag{12}$$

The corresponding result for TM modes is

$$k_{\rm f}h - \phi_{\rm c}^{\rm tm} - \phi_{\rm s}^{\rm tm} = m\pi, \tag{13}$$

which differs from eq. (12) only in that the correct phase shifts must be used for each polarization. The presence of the mode integer m is of central importance in these dispersion relations. Equations (7)–(9) and (11) show that for a given wavelength and set of refractive indices,  $k_f$  and the phase shifts are functions of the propagation constant  $\beta$ . Each value of m in either eq. (12) or (13), therefore, leads to a new value of  $\beta$ . The allowed values of  $\beta$  thus form a discrete set, not a continuum. Figure 10 shows the electric field profiles  $E_m(x)$  associated with the three lowest order TE modes of a typical planar waveguide. It is clear that the mode integer m determines the number of zero crossings that each mode exhibits. The same general behavior occurs for TM modes.

The careful reader might have noticed that the wave equations in eqs. (3) and (4) do not contain the  $\nabla \varepsilon$  terms ( $\varepsilon$  is the permittivity;  $\varepsilon = \varepsilon_0 n^2$ , with  $\varepsilon_0 = 8.85 \times 10^{-12}$  F/m) that appear for a medium in which the refractive index n depends on the coordinates [recall,  $n^2(x) = \varepsilon(x)/\varepsilon_0$ ]. Clearly, n = n(x) for the planar waveguide. This dependence can be made explicit by writing  $\varepsilon(x)$  in the form

$$\varepsilon(x) = \varepsilon_0 [n_s^2 + (n_f^2 - n_s^2) \theta(x) + (n_c^2 - n_f^2) \theta(x - h)], \qquad (14)$$

where  $\theta(x-a)$  is the unit step function, defined according to

$$\theta(x-a) = 0 \quad \text{for} \quad x < a ,$$
  
 
$$\theta(x-a) = 1 \quad \text{for} \quad x > a ,$$
 (15)

which shows explicitly the abrupt changes in  $\varepsilon$ , and hence  $n^2$ , at the boundaries of the waveguide. The more general wave equations are

$$\nabla^2 E + n^2(x) (\omega/c)^2 E = -\nabla \left\{ \frac{E \cdot \nabla \varepsilon}{\varepsilon} \right\}, \tag{16}$$

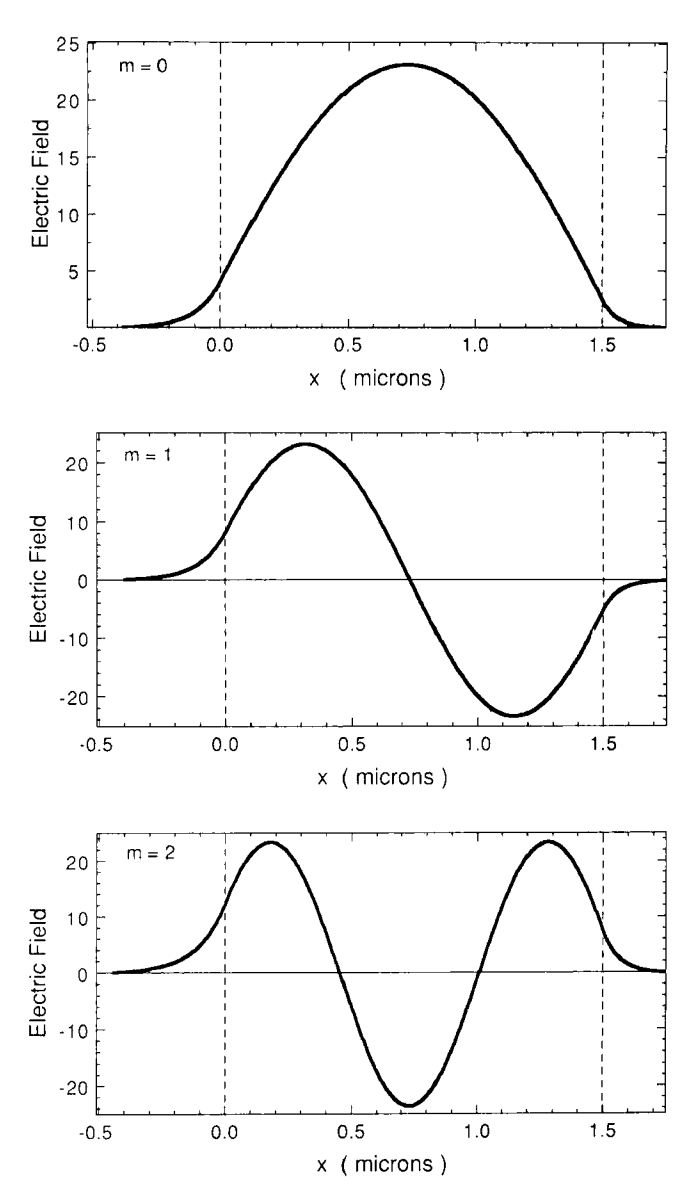


Fig. 10. Electric field distributions for the three lowest order TE modes for a planar optical waveguide of thickness  $h = 1.5 \, \mu \text{m}$  and  $n_s > n_c$ .

and

$$\nabla^2 H + n^2(x) (\omega/c)^2 H = i\omega(E \times \nabla \varepsilon). \tag{17}$$

When  $E_m(x)$  and  $H_m(x)$  in eqs. (5) and (6) are written in the style of eq. (14), it is not difficult to show that the previous solutions do indeed satisfy eqs. (16) and (17) as well as eqs. (3) and (4), as long as the boundary conditions on the tangential components of E and H are satisfied. More specifically, the delta-function terms generated by the  $\nabla^2$  operator and by  $\nabla \varepsilon$  can be made either to cancel or to vanish separately by applying the boundary conditions. The right-hand side of eq. (16), for example, vanishes for the TE modes of the planar waveguide, since the dot product  $E \cdot \nabla \varepsilon = 0$ .

It is conventional to introduce the effective index of refraction N, defined according to

$$N = \beta/k_0 \,, \tag{18}$$

where, again,  $k_0 = \omega/c = 2\pi/\lambda$ . One of the central properties of an optical waveguide is its ability to transport energy in a given direction, chosen to be the z-direction here. Since  $\beta$  is the z-component of the propagation constant, guided waves with field profiles such as those shown in fig. 10 can be said to propagate along z, treating the waveguide as a medium of refractive index N. It is easy to show that N is restricted to the range

$$n_{\rm s} \leqslant N \leqslant n_{\rm f} \,, \tag{19}$$

for bound modes, where it has been assumed that the substrate has the larger refractive index of the two outer media in fig. 1a:  $n_s \ge n_c$ . This refractive index convention will be adopted throughout this chapter. The effective index can be related to the propagation angle  $\theta$ , defined in a ray-optics model (see fig. 1a) as the angle between the ray and the normal, by the relation  $N = n_t \sin \theta$ , from which it is clear that the lower limit in eq. (19) represents the minimum value of  $\theta$  that provides total internal reflection at both interfaces. The upper limit in eq. (19) represents the natural limit  $\theta = \frac{1}{2}\pi$ . The dispersion relations in eqs. (12) and (13) can now be regarded as transcendental equations that determine N for guided waves of the TE and TM polarizations.

Figure 11 shows illustrative plots of the effective index N as a function of the film thickness h for both the m=0 and m=1 TE modes for a typical asymmetric geometry  $(n_s \neq n_c)$ . The parameters used for the plot are given in the figure caption. Typically, for a fixed wavelength and choice of refractive indices, there is a minimum thickness required to support a given mode of order m. For TE modes, for example, it is easy to show from eq. (12) that the minimum value

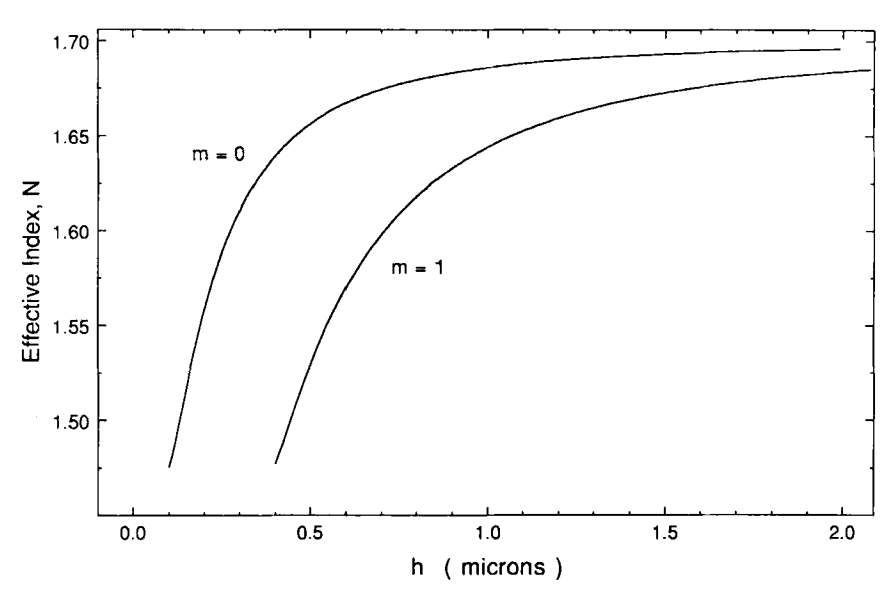


Fig. 11. Plots of the effective index of refraction N as a runction of the layer thickness h for the m=0 and m=1 modes of a sample optical waveguide, for which  $n_s=1.46$ ,  $n_f=1.7$ , and  $n_c=1$ .

of the ratio  $h/\lambda$ , the so-called cutoff value, for a guided wave of order m is given by

$$\left(\frac{h}{\lambda}\right)_{\min} = \frac{m\pi + \tan^{-1}\{\sqrt{a}\}}{2\pi\sqrt{n_{\rm f}^2 - n_{\rm s}^2}},\tag{20}$$

where

$$a = \frac{n_s^2 - n_c^2}{n_f^2 - n_s^2}. (21)$$

Inspection of eq. (20) shows that higher-order modes require thicker waveguides for propagation. Equation (20) also shows that for the case of a symmetric waveguide, for which  $n_s = n_c$  and a = 0, the ratio  $(h/\lambda)_{\min} = 0$ . This means that there is no nontrivial cutoff for the m = 0 mode of the symmetric optical waveguide. Equation (20) holds only for TE modes, but one obtains the same conclusion for TM modes. A symmetric waveguide of arbitrary nonzero thickness will support the m = 0 mode of both polarizations. This is analogous to the case of an optical fiber, a structure with refractive index confinement in

both transverse dimensions (x, y) and cylindrical symmetry, for which the lowest order mode also has no nontrivial cutoff.

One of the most important features to note in fig. 11 is that for a given waveguide with a given thickness h, the effective index N is different for the m = 0 and the m = 1 modes, even though the wavelength  $\lambda$  is the same for both modes. This is of central interest for efforts in the field of integrated optics, which attempts to define optical components such as lenses, gratings, switches, and modulators in or on optical waveguides. The effective index N determines the way in which a guided wave interacts with a component. If some of the incident energy in the waveguide is carried in each of the m = 0 and m = 1modes, then each mode will interact with the component in a different way to produce two different effects. In the case of a lens, for example, this means that there will be two different focal lengths. Other components have similar problems. It is for this reason that integrated optics is usually considered to be restricted to the use of single-mode waveguides. The presence of only one mode (of each polarization) in the waveguide permits a more precise definition of the operation of the components that make up an integrated optical or optoelectronic system.

A convenient normalization for the bound modes of the planar waveguide makes use of a power normalization. For the time dependence assumed here,  $\exp(-i\omega t)$ , the time-averaged Poynting vector S can be written as

$$S = \frac{1}{2} \operatorname{Re} \left\{ E \times H^* \right\}, \tag{22}$$

where Re designates the real part of the bracketed quantity and the asterisk designates the complex conjugate. The standard normalization sets to unity the power per unit width carried by the guided wave:

$$\int_{-\infty}^{\infty} \mathbf{S} \cdot \hat{\mathbf{z}} \, \mathrm{d}x = 1, \tag{23}$$

where the hat (^) designates a unit vector. For TE modes this reduces to

$$\frac{\beta}{2\mu_0\omega} \int_{-\infty}^{\infty} E_m(x) E_m^*(x) dx = 1 \quad \text{(TE)},$$

whereas for TM modes,

$$\frac{\beta}{2\omega} \int_{-\infty}^{\infty} \frac{H_m(x) H_m^*(x)}{\varepsilon(x)} dx = 1 \quad \text{(TM)},$$
 (25)

where  $\varepsilon(x)$  is as in eq. (14). The size of the planar waveguide is assumed to be

very large along the y-direction so that its size places no restrictions on the field distributions that can propagate. For this reason the integration in eq. (23) is carried out over only the x-dimension, and the result is referred to as the "power per unit width (along y)". In reality, eq. (23) is just a normalization condition.

The boundary conditions lead to relationships between the amplitude constants that appear in eqs. (6) and (10). For the TE case, for example, one obtains the following formulas

$$E_c^2 = E_f^2 \frac{n_f^2 - N^2}{n_f^2 - n_c^2}$$
 (TE), (26)

and

$$E_{\rm s}^2 = E_{\rm f}^2 \frac{n_{\rm f}^2 - N^2}{n_{\rm f}^2 - n_{\rm s}^2}$$
 (TE). (27)

These reduce the number of amplitude constants in eq. (6) from three to one, i.e.  $E_{\rm f}$ . When eq. (6) is inserted into the normalization integral in eq. (24),  $E_{\rm f}$  is then obtained in terms of the various waveguide parameters

$$1 = \frac{N}{4} \left(\frac{\varepsilon_0}{\mu_0}\right)^{1/2} E_f^2 h_{\text{eff}} \quad (\text{TE}) , \qquad (28)$$

where

$$h_{\text{eff}} = h + \frac{1}{\gamma_{c}} + \frac{1}{\gamma_{s}} \quad \text{(TE)}$$

is termed the effective waveguide thickness. Equation (28) determines the value of  $E_f$  subject to the normalization condition in eq. (23).

The TM result is a bit more complicated, but of the same form. The boundary conditions give

$$H_{c}^{2} = \frac{1}{q_{c}} \left( \frac{n_{c}^{2}}{n_{f}^{2}} \right) \frac{n_{f}^{2} - N^{2}}{n_{f}^{2} - n_{c}^{2}} H_{f}^{2} \quad (TM),$$
(30)

and

$$H_{\rm s}^2 = \frac{1}{q_{\rm c}} \left( \frac{n_{\rm s}^2}{n_{\rm c}^2} \right) \frac{n_{\rm f}^2 - N^2}{n_{\rm c}^2 - n_{\rm c}^2} H_{\rm f}^2 \quad (TM) \,, \tag{31}$$

where

$$q_i = (N/n_f)^2 + (N/n_i)^2 + 1 \quad (i = c, s),$$
 (32)

and the preceding notation follows that of KOGELNIK [1975]. The normalization integral, in turn, gives

$$1 = \frac{\frac{1}{4}N}{n_{\rm f}^2} \left(\frac{\mu_0}{\varepsilon_0}\right)^{1/2} H_{\rm f}^2 h_{\rm eff} \quad (TM) , \qquad (33)$$

where

$$h_{\text{eff}} = h + \frac{1}{\gamma_{c} q_{s}} + \frac{1}{\gamma_{s} q_{s}} \quad (TM).$$
 (34)

The mode functions also satisfy a useful orthogonality relation. For real refractive indices this relation is given by

$$\int_{-\infty}^{\infty} \left\{ E_{mt}(x) \times H_{nt}^{*}(x) \right\} \cdot \hat{\mathbf{z}} \, \mathrm{d}x = 0 \quad \text{for } m \neq n \,, \tag{35}$$

where the subscript t designates the *transverse* component of the vector field. Equation (35) can be applied to electric and magnetic fields of the forms given in eqs. (1) and (2), as long as one of them vanishes at  $x = \pm \infty$ . If one or both of them is a bound mode, this is certainly the case, not only for modes of the step-index planar waveguide, but also for more complicated structures such as planar, graded-index optical waveguides. It is only necessary that eqs. (1) and (2) describe the fields and that they behave properly at  $x = \pm \infty$ .

## 3.2. BOUND MODES OF THE GRADED-INDEX OPTICAL WAVEGUIDE

One often encounters optical waveguides for which the refractive index is a continuous function of at least one of the spatial coordinates. Such waveguides are called graded-index waveguides. A sketch of the simplest type of a planar, graded-index waveguide, for which  $n_{\rm f}$  depends on the single coordinate x, appears in fig. 12. Note that x increases downward from the upper waveguide surface in fig. 12, in contrast to fig. 1. In this structure the refractive index  $n_{\rm f}(x)$  is greatest at x=0 and diminishes with increasing x until it reaches some constant value. In practice, waveguides of this type are often made by diffusing some species into a host crystal. The result is a region typically a few microns thick for which the average refractive index exceeds the ambient value in the

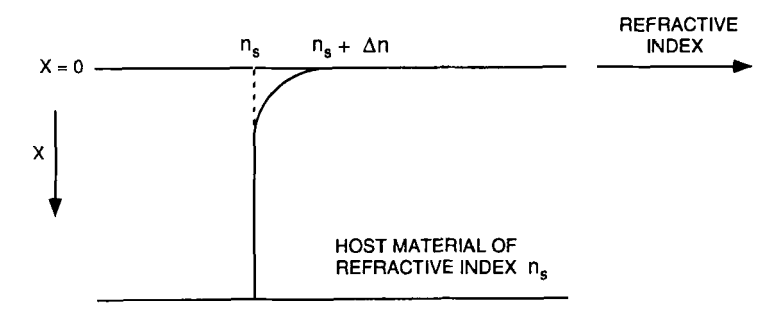


Fig. 12. The geometry for a typical graded-index optical waveguide. The refractive index is highest at the surface and decreases with depth toward the ambient value of the most material.

host crystal. This higher-index region can confine light in much the same way as the step-index structure.

The qualitative features of the bound modes of the graded-index waveguide are not significantly different from those of the step-index waveguide. Electric and magnetic fields of the form given in eqs. (1) and (2) solve the wave equations in eqs. (16) and (17), subject to the appropriate boundary conditions. The graded-index waveguide supports both TE and TM modes, but the mode functions  $E_m(x)$  and  $H_m(x)$  are more complicated than those for the step-index waveguide. It is usually the case that both the mode functions and the dispersion relations can only be determined by numerical techniques. A discussion of these techniques is outside the scope of this chapter, but the reader can consult the published literature for further information. (Conwell [1973], Kogelnik [1975], Korotky and Alferness [1987], Hocker and Burns [1975]).

#### 3.3. BOUND MODES OF THE NONLINEAR OPTICAL WAVEGUIDE

Certain materials exhibit a type of nonlinear response that leads to a refractive index that depends on the intensity of the optical wave propagating in the medium. If the wave has a nonuniform spatial profile, it produces an index gradient that, in turn, modifies the properties of the propagating wave. The self-focusing of a laser beam in a nonlinear medium is perhaps the most familiar example of this process.

A layer of this nonlinear material, bounded by linear media, is capable of supporting guided waves. An exhaustive discussion of this subject is beyond

the scope of this chapter, but one example will be examined here. Equation (36) gives the refractive index configuration for this example,

$$n^{2}(x) = n_{c}^{2} \qquad x > h,$$

$$= n_{s}^{2} + \Delta + n_{2} |E|^{2} \quad 0 < x < h,$$

$$= n_{s}^{2} \qquad x < 0.$$
(36)

Here,  $n_2$  is the nonlinear coefficient that describes the (real) magnitude of the nonlinear term in the refractive index of the layer and  $\Delta$  is a small, negative (real) number. For E = 0, the refractive index of the layer is smaller than that of the substrate  $(n_s)$ , which means that the layer cannot serve as an optical waveguide in the conventional sense, since the total internal reflection condition cannot be satisfied at both interfaces. As E grows, the nonlinear term will first equal, then exceed  $\Delta$ , and one expects bound modes of some sort to appear.

The wave equation for TE modes can be solved using the familiar form

$$E = \hat{\mathbf{y}} G(x) e^{i(\beta z - \omega t)}, \tag{37}$$

where

$$G(x) = E_{c} e^{-\gamma_{c}(x-h)} \qquad x > h,$$

$$= E_{f} \operatorname{sech} \{k_{f}(x-x_{0})\} \quad 0 < x < h,$$

$$= E_{s} e^{\gamma_{s}x} \qquad x < 0.$$
(38)

is the mode profile. Application of the boundary conditions on the tangential components of the electric and magnetic fields leads to the dispersion relation

$$\tanh(k_{\rm f}h) = \frac{k_{\rm f}(\gamma_{\rm c} + \gamma_{\rm s})}{k_{\rm f}^2 + \gamma_{\rm c}\gamma_{\rm c}}.$$
 (39)

It is convenient at this point to introduce a few new parameters in terms of which to discuss some interesting features of these nonlinear guided waves. The parameters V, D, and a are defined according to

$$V = \left(\frac{2\pi h}{\lambda}\right) |\Delta|^{1/2},\tag{40}$$

$$D = \frac{n_2 E_{\rm f}^2}{2|\Delta|} - 1, \tag{41}$$

$$a = \frac{(n_{\rm s}^2 - n_{\rm c}^2)}{|\Delta|}. (42)$$

The original parameters can be expressed in terms of the new ones as:

$$k_{\rm f} = k_0 \{ |\Delta| \, (1+D) \}^{1/2} \,, \tag{43}$$

$$\gamma_{c} = k_{0} \{ |\Delta| (D+a) \}^{1/2}, \tag{44}$$

$$\gamma_{\rm s} = k_0 (|\Delta| D)^{1/2} \,. \tag{45}$$

The dispersion relation can therefore be written in the form

$$\tanh\{V\sqrt{1+D}\} = \frac{\sqrt{1+D}(\sqrt{D}+\sqrt{D+a})}{1+D+\sqrt{D}\sqrt{D+a}}.$$
 (46)

The exponential decay rates in eqs. (44) and (45) must be positive to assure proper behavior at  $x = +\infty$ . This is only possible for  $D \ge 0$ , which means that the minimum power the wave must carry is determined from the condition

$$(E_{\rm f}^2)_{\rm minimum} = \frac{2|\Delta|}{n_2},\tag{47}$$

which is a condition that ultimately determines the required minimum intensity of the source used to excite the nonlinear guided wave. The larger the nonlinear coefficient, the smaller the required intensity. The effective index of refraction  $N = \beta/(\omega/c)$ , introduced earlier, is "power dependent" for the nonlinear wave and is given by

$$N = (n_s^2 + |\Delta| D)^{1/2}. (48)$$

As in the discussion of the step-index waveguide, N must exceed  $n_s$ , which follows immediately from eq. (48) and the condition  $D \ge 0$ . This suggests a connection with the normal internal reflection mechanism that is at work in the step-index case.

The dispersion relation provides the allowed values of N for a given structure and choice of wavelength or frequency. Figure 13 shows a plot of the dispersion relation from eq. (46), plotted as N versus V, since D determines N according to eq. (48), for a symmetric structure (a = 0). It is significant that for a given V, i.e. a given structure, there are two distinct solutions for N, and hence for D, for a given value of V. This result means that two different nonlinear guided waves can, in principle, be supported by a particular nonlinear waveguide at two different power levels.

There are other structures that support nonlinear guided waves. For example, a nonlinear waveguide can be formed by depositing a layer of a linear material onto a nonlinear substrate, or by sandwiching a linear layer between two

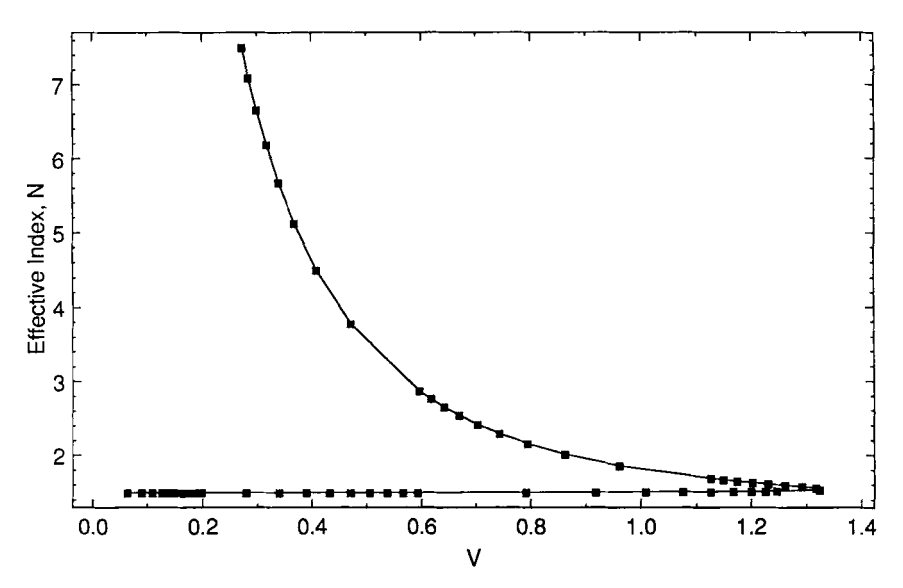


Fig. 13. Plot of the effective index N as a function of the parameter V for the nonlinear optical waveguide.

nonlinear media. Furthermore, important issues such as the stability of the nonlinear waves and the means of exciting these waves remain the subjects of very active investigation. The reader is referred to the extensive literature on nonlinear waveguides for more exhaustive treatments of the subject (STEGEMAN, BURKE and SEATON [1987]).

#### 3.4. RADIATION MODES OF THE STEP-INDEX WAVEGUIDE

The previous sections described the bound modes that are supported by planar optical waveguide structures of various kinds, with emphasis on the step-index waveguide. The TE and TM modes were described by electric and magnetic fields of the form

$$\boldsymbol{E} = \hat{\mathbf{y}} E_{y}(x) e^{i(\beta z - \omega t)} \quad \text{and} \quad \boldsymbol{H} = \hat{\mathbf{y}} H_{y}(x) e^{i(\beta z - \omega t)}, \tag{49}$$

which vanishes at  $\pm \infty$ , and for which  $n_s(\omega/c) \le \beta \le n_f(\omega/c)$ . The wave equations also admit solutions of the form given in eq. (49) for other values of (real)  $\beta$ , but they are not localized near the waveguide layer. These solutions are termed radiation modes and correspond to oscillating fields in at least two

of the three media in fig. 1a. Since they have the form of eq. (49), the radiation modes of the step-index waveguide are orthogonal to the bound modes of the same waveguide, according to eq. (35), although they cannot be normalized by the simple prescription in eq. (23). Only the essential characteristics of the radiation modes will be described here.

The two types of radiation modes for the geometry in fig. 1a are substrate radiation modes and substrate-cover radiation modes. Retaining the usual convention that  $n_{\rm s} \geqslant n_{\rm c}$ , for the substrate radiation modes,  $\beta$  is restricted to the range  $n_{\rm c} k_0 \leqslant \beta \leqslant n_{\rm s} k_0$ . The field profiles for the TE and TM substrate modes are

$$E_{y}(x) = E_{c} e^{-\gamma_{c}(x-h)} \qquad x > h ,$$

$$= E_{f} \cos \{q_{f}(x-h) + \phi_{c}^{(e)}\} \quad 0 < x < h ,$$

$$= E_{s} \cos (q_{s} x + \phi^{(e)}) \qquad x < 0 ,$$
(50)

and

$$H_{y}(x) = H_{c} e^{-\gamma_{c}(x-h)} \qquad x > h ,$$

$$= H_{f} \cos \left\{ q_{f}(x-h) + \phi_{c}^{(m)} \right\} \quad 0 < x < h ,$$

$$= H_{s} \cos \left( q_{s} x + \phi^{(m)} \right) \qquad x < 0 , \qquad (51)$$

where each is in a form consistent with that used by KOGELNIK [1975]. It is clear from the field profiles and the range of  $\beta$  considered that a substrate radiation mode has total internal reflection at the cover/film boundary (x = h), but not at the substrate/film boundary (x = 0). In fact, eqs. (50) and (51) are precisely the fields one obtains by solving the Fresnel reflection problem for the case of a plane wave incident on the film layer from the substrate at an angle greater than or equal to  $\theta = \arcsin(n_c/n_s)$ , measured with respect to the normal. It is important to note that  $\beta$  is continuous within its prescribed range for radiation modes, as one might expect given the analogy with the Fresnel reflection problem.

The situation is more complicated for the substrate-cover radiation modes, for which  $0 \le \beta \le n_c k_0$ . There are two sets of these radiation modes, which can be understood by noting that for a symmetrical waveguide the field profiles will possess even or odd symmetry. For the asymmetric waveguide one set of radiation modes must possess even symmetry and the other, odd symmetry, in the limit  $n_s \to n_c$ . The field profiles for the TE and TM substrate-cover modes

are of the form

$$E_{y}(x) = E_{c}^{\pm} \frac{\cos}{\sin} \left\{ q_{c}(x - h) + c_{\pm}^{(e)} \right\} \qquad x > h,$$

$$= E_{f}^{\pm} \frac{\cos}{\sin} \left\{ q_{f}x - \alpha^{(e)} \right\} \qquad 0 < x < h,$$

$$= E_{s}^{\pm} \frac{\cos}{\sin} \left( q_{s}x - s_{\pm}^{(e)} \right) \qquad x < 0,$$
(52)

and

$$H_{y}(x) = H_{c}^{\pm} \frac{\cos}{\sin} \left\{ q_{c}(x - h) + c_{\pm}^{(m)} \right\} \quad x > h ,$$

$$= H_{f}^{\pm} \frac{\cos}{\sin} \left\{ q_{f}x - \alpha^{(m)} \right\} \qquad 0 < x < h ,$$

$$= H_{s}^{\pm} \frac{\cos}{\sin} \left( q_{s}x - s_{\pm}^{(m)} \right) \qquad x < 0 , \tag{53}$$

where, in each expression, e and m label TE- and TM-related quantities, + and - designate even and odd modes, respectively, and cosine is used for even (+) modes, sine is used for odd (-) modes. Physically, these modes correspond to spatially oscillating fields in all three media. They can be viewed as properly phased superpositions of the solutions to the Fresnel reflection problem for the cases of plane waves incident upon the layer of thickness h from above and below.

Although this will not be discussed in detail at this point, the bound and radiation modes of the step-index planar optical waveguide constitute a complete set of orthogonal functions. The bound modes make up the discrete spectrum, and the radiation modes make up the continuous spectrum. It is often convenient to use a mode expansion based on these functions when analyzing interactions in optical waveguides that have been perturbed in some fashion. A typical example is a waveguide with one corrugated surface. The periodic surface perturbation can provide a mechanism for converting forwardgoing waves into backward-going waves, or for coupling the bound modes with the radiation field, as might be exploited for input or output coupling.

Since the major emphasis in this chapter, the interaction between bound

modes and waveguide gratings, does not require a deep understanding of the radiation modes, no further details about them are given here. The interested reader is referred to the works of KOGELNIK [1975] and MARCUSE [1974].

## § 4. Nonplanar Optical Waveguides

The waveguide geometries so far considered in this chapter provide confinement along only a single coordinate axis. Waveguides that provide confinement along two axes are required for several applications. The circularly cylindrical optical fiber is the most familiar example, but other types are in common use as well. Unfortunately, numerical techniques are needed to analyze these structures in detail, but their qualitative features are easy to infer from those obtained earlier for planar waveguides.

The fields associated with the bound modes of the three-dimensional waveguide are of the general form

$$E(x, y, z, t) = \hat{\mathbf{y}} E_{mn}(x, y) e^{i(\beta_{mn}z - \omega t)}, \qquad (54)$$

and

$$H(x, y, z, t) = \hat{y} H_{mn}(x, y) e^{i(\beta_{mn}z - \omega t)},$$
 (55)

for assumed propagation along the z-direction. Note that the propagation constant  $\beta$  now depends on the two mode integers m and n, and that the field amplitudes depend on both the x- and y-coordinates. When the size of the waveguide is sufficiently small along each of the two transverse directions, a standing wave is set up within the guiding region much like the case for one-dimensional confinement. This leads to field distributions much like those shown in fig. 10 along each transverse direction. Only one integer label was needed in the case of the planar waveguide, an integer that specifies the number of zeros of the field. Two such integers are needed for confinement along two axes, since the number of zero-crossings need not be the same in both directions. Strictly speaking, the x- and y-dependences in eqs. (54) and (55) are not separable, although it is sometimes a useful approximation to write

$$E_{mn}(x, y) \approx f_m(x) g_n(y), \qquad (56)$$

and likewise for the magnetic field.

The modes satisfy a dispersion relation that involves the two mode integers m and n. They also satisfy an orthogonality relation given by

$$\int_{-\infty}^{\infty} \int_{-\infty}^{\infty} \left\{ E_{mqt}(x) \times H_{nst}^{*}(x) \right\} \cdot \hat{\mathbf{z}} \, \mathrm{d}x \, \mathrm{d}y = 0 \quad \text{for } m \neq n \text{ and } q \neq s \,, \tag{57}$$

where the subscript t, again, designates the transverse component(s) of the field, just as in eq. (35) for planar waveguides. The notation (three subscripts) is somewhat cumbersome, but eq. (57) is just the natural extension of the earlier result.

This chapter does not make use of the detailed forms of the modes supported by the two-dimensional waveguide, so no further discussion of them is included here. The interested reader can consult the references for further information (ADAMS [1981], KOGELNIK [1988]).

## § 5. Coupling Between Guided Waves

The problem of a guided-wave propagating in a periodic medium can be formulated in a variety of ways. Of particular interest is the case for which the propagation constant  $\beta$  (along z) very nearly satisfies the Bragg condition. The most popular theoretical technique develops a pair of coupled-mode equations that connect the amplitudes of the forward- and backward-propagating waves. These equations can be extracted directly from the one-dimensional wave equation, as demonstrated below.

Consider the following one-dimensional differential equation:

$$\left[\frac{\mathrm{d}^2}{\mathrm{d}z^2} + \beta^2\right] f(z) = -2\beta K(z) f(z), \qquad (58)$$

where the specific choice of constants on the right-hand side has been chosen for convenience. The important feature of the right-hand side of the equation is the product form; K(z) is simply some function of z. A particular solution of eq. (58) can be written in terms of a Green function g(z, z') for the one-dimensional Helmholtz equation according to

$$f(z) = \int_{-\infty}^{\infty} g(z, z') \left[ -2\beta K(z') f(z') \right] dz', \qquad (59)$$

where g(z, z') for the one-dimensional Helmholtz equation is known to be

$$g(z,z') = \frac{e^{i\beta|z-z'|}}{2i\beta},\tag{60}$$

subject to the requirement that only outgoing waves appear at  $z \to +\infty$ . [Recall the time dependence used here is  $\exp(-i\omega t)$ .]

To simplify what follows it is convenient to define the right-hand side of eq. (58) as Q(z),

$$Q(z) = -2\beta K(z) f(z). \tag{61}$$

The absolute value in eq. (60) makes it clear that eq. (59) can be written as the sum of two terms, one for z' > z and one for z' < z,

$$f(z) = A^{+}(z) e^{i\beta z} + A^{-}(z) e^{-i\beta z}, \qquad (62)$$

where  $A^+$  and  $A^-$  are the z-dependent amplitudes of forward-going and backward-going waves, respectively, given by

$$A^{+}(z) = \frac{1}{2i\beta} \int_{-\infty}^{z} e^{-i\beta z'} Q(z') dz', \qquad (63)$$

and

$$A^{-}(z) = \frac{1}{2i\beta} \int_{z}^{\infty} e^{i\beta z'} Q(z') dz'.$$
 (64)

It is now easy to show that eqs. (63) and (64) correspond to a set of coupled, first-order differential equations that determine the amplitudes  $A^+$  and  $A^-$ . First, differentiate eqs. (63) and (64) to obtain

$$\frac{\mathrm{d}A^{+}}{\mathrm{d}z} = \frac{1}{2\mathrm{i}\beta} \,\mathrm{e}^{-\mathrm{i}\beta z} \,Q(z)\,,\tag{65}$$

and

$$\frac{\mathrm{d}A^{-}}{\mathrm{d}z} = -\frac{1}{2\mathrm{i}\beta} \,\mathrm{e}^{\mathrm{i}\beta z} \,Q(z) \,. \tag{66}$$

Next, substitute eqs. (61) and (62) into eqs. (65) and (66). The results have the simple form

$$\frac{dA^{+}}{dz} = iK(z)A^{+}(z) + iK(z)A^{-}(z)e^{-i2\beta z}, \qquad (67)$$

and

$$\frac{dA^{-}}{dz} = -iK(z)A^{+}(z)e^{i2\beta z} - iK(z)A^{-}(z).$$
 (68)

These are the coupled-amplitude, or coupled-mode, equations.

Equation (58) contains no dependence on the transverse coordinates, something that is essential for a proper description of interactions in an optical waveguide. The wave equation, however, often reduces to that in eq. (58) within some convenient approximation that allows integration over the transverse coordinate(s). As soon as such an integration becomes possible, coupled equations of the form given in eqs. (67) and (68) can be expected to emerge from the analysis.

Several treatments of the problem of grating coupling between guided waves will be presented and discussed here. Not all of these start with the wave equation, but coupled amplitude equations of the form that appears in eqs. (67) and (68) nevertheless emerge from all these analyses.

#### 5.1. IDEAL-MODE EXPANSION AND COUPLED-MODE EQUATIONS

Most of the published coupled-mode formulations of the problem of the interaction of a guided wave with a waveguide grating have been based on the so-called *ideal-mode* expansion. Slightly different versions of this approach to the grating problem have been used by Yariv [1973], Marcuse [1974], Kogelnik [1975], Streifer, Scifres and Burnham [1975], Wagatsuma, Sakaki and Saito [1979], and others (Yamamoto, Kamiya and Yanai [1978], Lin, Zhou, Chang, Fououhar and Delavaux [1981]). All versions of the theory provide a good description for TE-polarized guided waves, but there is evidence that the approach fails for the TM polarization. Kogelnik's [1975] treatment is particularly instructive, and is included here to illustrate the *ideal-mode* technique. Only planar waveguides are considered.

The transverse (to z) components of the waveguide mode functions form a complete set of orthonormal functions that can serve as the basis set for an expansion of the fields of interest. This is true strictly for real refractive indices and real values of the propagation constant  $\beta$ . The expansion includes both bound and radiation modes. If  $E_t$  and  $H_t$  represent the transverse components of the fields of interest for a forward-going wave (propagating in the +z direction), the mode expansion can be written as

$$E_{t}^{+} = \sum_{n} a_{n}^{+}(z) E_{nt}^{(i)}(x) + \int_{0}^{\infty} a^{+}(z;q) E_{t}^{(i)}(x;q) dq, \qquad (69)$$

and

$$H_{t}^{+} = \sum_{n} a_{n}^{+}(z) H_{nt}^{(i)}(x) + \int_{0}^{\infty} a^{+}(z;q) H_{t}^{(i)}(x;q) dq.$$
 (70)

The superscript + designates a forward-going wave, the superscript (i) designates a mode of the ideal waveguide. In each of the above equations there is a discrete sum over the bound modes and a continuous one, expressed as an integral, over the radiation modes. The quantity q in the latter represents the spatial frequency associated with radiation in a given direction. The expansion "coefficients",  $a_n(z)$  and a(z), depend on z. The expansion is based on the idea that the fields of interest can be expanded in the modes of a particular unperturbed waveguide, the ideal waveguide, for which the modes are known and given by eqs. (6), (10), (50), and (51). The superscript (i) is assigned here to make the identification of an ideal mode as clear as possible. The form written in eqs. (69) and (70) assumes that each term in the expansion can be factored into a product that separates the x- and z-dependence. In what follows, a somewhat simpler notation will be used to represent the mode expansions in eqs. (69) and (70). Namely, a single summation symbol will be used to represent both the discrete and the continuous sums in the mode expansions. The emphasis here is on the bound modes, but Kogelnik's formalism applies equally well to the radiation modes.

An alternative expansion, the *local* normal mode (LNM) expansion, to be discussed later, is based on a different idea. At each z the fields are expanded in terms of the modes of the unperturbed waveguide with the local thickness. This means that in the LNM expansion, the modal fields depend on z, since the perturbed waveguide has a thickness that varies with z. The results of the two types of expansions do not always agree.

KOGELNIK [1975] examines the problem of a guided-wave propagating along the z-direction, perpendicular to the "rulings" of a surface grating that is very nearly of the correct period for Bragg reflection (see, e.g. fig. 5). The grating is presumed to be very wide so that the fields exhibit no y-dependence. The development of the basic equations of the ideal-mode approach proceeds as follows. Consider an unperturbed waveguide with permittivity  $\varepsilon(x) = n^2(x)\varepsilon_0$  [see eq. (5)]. This waveguide structure is then perturbed, by corrugating one interface, e.g., so that the permittivity becomes  $\varepsilon(x) + \Delta \varepsilon(x, z)$ ; the specific details about the corrugation are contained in  $\Delta \varepsilon(x, z)$ . Maxwell's two curl equations for the fields of the perturbed structure are [assume  $\exp(-i\omega t)$ ]

$$\mathbf{V} \times \mathbf{E} = \mathrm{i}\mu\omega\mathbf{H}\,,\tag{71}$$

and

$$\nabla \times \boldsymbol{H} = -i\omega(\varepsilon + \Delta\varepsilon)\boldsymbol{E} \,. \tag{72}$$

Let the subscripts 1 and 2 refer to two waves, each of which is described by fields that satisfy eqs. (71) and (72) for either  $\Delta \varepsilon = 0$  (the ideal waveguide) or  $\Delta \varepsilon \neq 0$ . If wave 2 propagates in the ideal waveguide and wave 1 propagates in the perturbed waveguide, it is straightforward to show that

$$\nabla \cdot (E_1 \times H_2^* + E_2^* \times H_1) = i\omega(\Delta \varepsilon) E_1 \cdot E_2^*, \tag{73}$$

where the complex conjugates of eqs. (71) and (72) have been used.

Next, integrate eq. (73) over x and separate the z-derivative from the x-derivative on the left-hand side of the resulting equation,

$$\int_{-\infty}^{\infty} \left( \hat{\mathbf{x}} \frac{\partial}{\partial x} + \hat{\mathbf{z}} \frac{\partial}{\partial z} \right) \cdot (E_1 \times H_2^* + E_2^* \times H_1) \, \mathrm{d}x = \mathrm{i}\omega \int_{-\infty}^{\infty} (\Delta \varepsilon) E_1 \cdot E_2^* \, \mathrm{d}x \,. \tag{74}$$

The integration over the  $\partial/\partial x$  term vanishes if either or both of waves 1 or 2 is a bound mode, since the fields for a bound mode vanish at  $x = \pm \infty$ . Wave 2, by hypothesis, has fields of the form given in eq. (1) and (2); assume for the moment that this is a forward-going wave:

$$\boldsymbol{E}_2 = \hat{\mathbf{y}} E_m^{(i)}(x) \exp\left[i(\beta z - \omega t)\right] \quad \text{and} \quad \boldsymbol{H}_2 = \hat{\mathbf{y}} H_m^{(i)}(x) \exp\left[i(\beta z - \omega t)\right]. \tag{75}$$

The fields for wave 1 can be expanded according to eqs. (69) and (70), the ideal-mode expansion, after one small change. Since  $E_2$  and  $H_2$  will both contain forward- and backward-going waves due to the Bragg interaction, terms must be added to eqs. (69) and (70) to represent the latter. The replacements

$$a_n^+(z) \to a_n^+(z) + a_n^-(z)$$
 and  $a^+(z;q) \to a^+(z;q) + a^-(z;q)$  (76)

in eq. (69), along with

$$a_n^+(z) \to a_n^+(z) - a_n^-(z)$$
 and  $a^+(z;q) \to a^+(z;q) - a^-(z;q)$  (77)

in eq. (70), make it explicit that both forward-going (+) and backward-going (-) waves are included, and make sure that the direction of Poynting's vector  $E \times H$  is correct in both cases ( $H_t$  changes sign for a backward-going wave;  $E_t$  does not).

The use of the orthogonality relation (recall that the bound modes are orthogonal to the radiation modes), eq. (35), after these substitutions in eq. (74) gives the result

$$\frac{\mathrm{d}a_m^+(z)}{\mathrm{d}z} - \mathrm{i}\beta_m a_m^+(z) = \frac{1}{4} \mathrm{i}\omega \int_{-\infty}^{\infty} (\Delta \varepsilon) \boldsymbol{E}_1 \cdot \{\boldsymbol{E}_m^{(i)\,+}\}^* \,\mathrm{d}x \,. \tag{78}$$

Had wave 2 been chosen to be a backward-going wave, the result would have been

$$\frac{\mathrm{d}a_m^-(z)}{\mathrm{d}z} + \mathrm{i}\beta_m a_m^-(z) = -\frac{1}{4}\mathrm{i}\omega \int_{-\infty}^{\infty} (\Delta \varepsilon) \boldsymbol{E}_1 \cdot \{\boldsymbol{E}_m^{(\mathrm{i})}^-\} * \mathrm{d}x, \qquad (79)$$

where the superscripts + and - designate quantities associated with forwardand backward-going waves. These can be further reduced by introducing the amplitudes  $A^+(z)$  and  $A^-(z)$ ,

$$a_m^+(z) = A_m^+(z) \exp(i\beta z)$$
 and  $a_m^-(z) = A_m^-(z) \exp(-i\beta z)$ , (80)

with the results

$$\frac{\mathrm{d}A_m^+(z)}{\mathrm{d}z} = \frac{1}{4}\mathrm{i}\omega \int_{-\infty}^{\infty} (\Delta\varepsilon) E_1 \cdot \{E_m^{(i)+}\}^* \,\mathrm{d}x\,,\tag{81}$$

and

$$\frac{\mathrm{d}A_m^-(z)}{\mathrm{d}z} = -\frac{1}{4}\mathrm{i}\omega \int_{-\infty}^{\infty} (\Delta\varepsilon) E_1 \cdot \{E_m^{(i)-}\}^* \,\mathrm{d}x \,. \tag{82}$$

The transverse component of the field  $E_1$  that appears on the right-hand side of these equations can be expanded in the same way as described above, using eqs. (69) and (76), but the z-component is handled differently in Kogelnik's treatment. It is easy to show that  $H_{1t}$  and  $E_{1z}$  are related according to

$$\nabla_{t} \times H_{1t} = -i\omega(\varepsilon + \Delta \varepsilon) E_{1z}. \tag{83}$$

 $H_{1t}$  can be expanded using eqs. (70) and (77), which means that eq. (83) can be used to determine an expansion for  $E_{1z}$ . The result is

$$\boldsymbol{E}_{1z} = \frac{\varepsilon}{\varepsilon + \Delta\varepsilon} \sum_{m} \left\{ a_{m}^{+}(z) - a_{m}^{-}(z) \right\} \boldsymbol{E}_{mz}^{(i)}(x) . \tag{84}$$

It is convenient to define two quantities that describe the interaction in the waveguide,

$$K_{mn}^{t}(z) = \frac{1}{4}\omega \int_{-\infty}^{\infty} (\Delta\varepsilon) E_{mt}^{(i)} \cdot \{E_{nt}^{(i)}\}^* dx, \qquad (85)$$

and

$$K_{mn}^{z}(z) = \frac{1}{4}\omega \int_{-\infty}^{\infty} \left(\frac{\varepsilon \Delta \varepsilon}{\varepsilon + \Delta \varepsilon}\right) E_{mz}^{(i)} \cdot \{E_{nz}^{(i)}\}^{*} dx.$$
 (86)

The superscripts + and - have been dropped from the modal fields in eqs. (85) and (86), since the signs used with  $a_n(z)$  [see eqs. (76) and (77)] in the mode expansion ensure the proper choice of signs for forward- and backward-going waves. The right-hand sides of the coupled-mode equations, eqs. (81) and (82), can now be expanded according to eqs. (69), (76), and (84) to obtain

$$\frac{\mathrm{d}A_{n}^{+}}{\mathrm{d}z} = \mathrm{i} \sum_{m} \left[ A_{m}^{+} \left( K_{mn}^{t} + K_{mn}^{z} \right) \mathrm{e}^{\mathrm{i}(\beta_{m} - \beta_{n})z} + A_{m}^{-} \left( K_{mn}^{t} - K_{mn}^{z} \right) \mathrm{e}^{-\mathrm{i}(\beta_{m} + \beta_{n})z} \right],$$
(87)

and

$$\frac{dA_{n}^{-}}{dz} = -i \sum_{m} \left[ A_{m}^{+} (K_{mn}^{t} - K_{mn}^{z}) e^{i(\beta_{m} + \beta_{n})z} + A_{m}^{-} (K_{mn}^{t} + K_{mn}^{z}) e^{i(\beta_{m} - \beta_{n})z} \right].$$
(88)

These are the coupled-mode equations as derived by KOGELNIK [1975] for the two-dimensional case (no y-dependence). Once the perturbation  $\Delta \varepsilon$  has been defined, the quantities in eqs. (85) and (86) can be determined, since the ideal modes are known, and the system of coupled differential equations in eqs. (87) and (88) can be solved, at least in principle.

Figure 14 shows a typical perturbed waveguide structure, a segment of a waveguide with a cosine corrugation on the upper surface. The unperturbed,

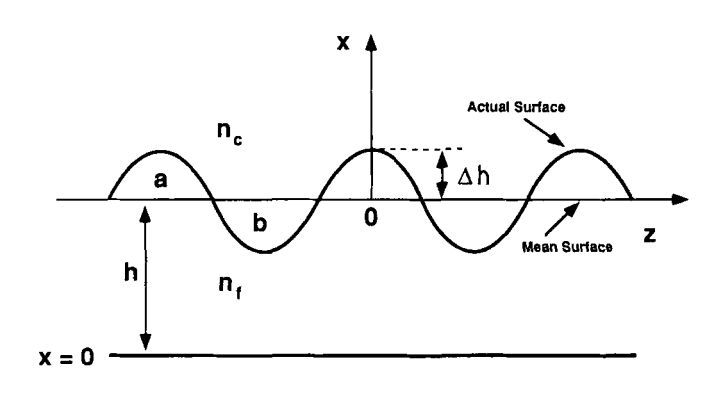


Fig. 14. A planar optical waveguide with a corrugated upper surface. The surface grating is made up of two perturbation regions, labeled a and b. The grating depth is  $2 \Delta h$ ; the ratio  $\Delta h/h$  is taken to be small. The grating has a period  $\Lambda$ .

n,

or ideal, waveguide is taken to be the mean waveguide of thickness h shown in the figure. The location of the upper surface x = d of the perturbed, or actual, waveguide is given by

$$d = h + \Delta h \cos(K_0 z), \tag{90}$$

where  $\Delta h$  gives the strength of the grating and  $K_0 = 2\pi/\Lambda$  is the grating constant, with  $\Lambda$  the grating period. The permittivity  $\varepsilon(x) = n^2(x)\varepsilon_0$  for the unperturbed waveguide appears in eq. (5). The perturbation  $\Delta \varepsilon(x, z)$  is the difference between the permittivities of the actual and ideal waveguides,

$$\Delta \varepsilon = \varepsilon_0 (n_{\rm f}^2 - n_{\rm c}^2) \quad h < x < d, \quad \text{as for region a,}$$

$$= \varepsilon_0 (n_{\rm c}^2 - n_{\rm f}^2) \quad d < x < h, \quad \text{as for region b.}$$
(91)

The expressions in eqs. (85) and (86) can be evaluated very simply for the case of a small corrugation depth and TE polarization for both the forward-going and backward-going waves, for which  $K_{mn}^z(z) = 0$ . We find, e.g., for m = n = 0,

$$K_{00}^{\mathsf{t}}(z) = 2\kappa \cos(K_0 z), \tag{92}$$

where

$$\kappa = \frac{\pi}{\lambda} \frac{\Delta h}{h_{\text{eff}}} \frac{n_{\text{f}}^2 - N^2}{N} \quad \text{(TE-TE)} \,. \tag{93}$$

In the above equations the normalization condition in eq. (24) has been used, along with eq. (29);  $\kappa$  is referred to as the coupling coefficient.

The corresponding expression for the coupling coefficient  $\kappa$  for TM-polarized waves that emerges from Kogelnik's treatment is

$$\kappa = \frac{\pi}{\lambda} \frac{\Delta h}{h_{\text{eff}}} \frac{n_{\text{f}}^2 - N^2}{N} \left[ \left\{ \frac{1}{2q_{\text{c}}} \left( \frac{n_{\text{f}}^2}{n_{\text{c}}^2} + \frac{n_{\text{c}}^2}{n_{\text{f}}^2} \right) \right\} \left( \frac{N^2}{n_{\text{f}}^2} - \frac{N^2}{n_{\text{c}}^2} + 1 \right) \right]$$
(7M-TM),

where  $q_c$  was defined in eq. (32), and the values of N and  $h_{\rm eff}$  appropriate for TM modes must be used [see eq. (34)]. There is strong evidence that eq. (93) is correct and eq. (94) is *incorrect*, as will be discussed later in this chapter. It appears that the correct TM-TM result can be obtained by setting the quantity in curly brackets  $\{ \}$  to unity in eq. (94).

The number of terms that must be retained in eqs. (87) and (88) to provide an acceptable quantitative description for a given situation is a matter of great importance. If we consider a waveguide that is sufficiently thin so that it supports only the lowest order TE mode, we can assume that all the amplitudes are zero except n = 0:

$$A_n^+(z) = A_n^-(z) = 0 \quad \text{for } n \neq 0.$$
 (95)

The coupled-mode equations then reduce to

$$\frac{\mathrm{d}A_0^+}{\mathrm{d}z} = \mathrm{i}A_0^+ K_{00}^t + \mathrm{i}A_0^- K_{00}^t \,\mathrm{e}^{-\mathrm{i}2\beta_0 z}\,,\tag{96}$$

and

$$\frac{\mathrm{d}A_0^-}{\mathrm{d}z} = -\mathrm{i}A_0^+ K_{00}^t \,\mathrm{e}^{\mathrm{i}2\beta_0 z} - \mathrm{i}A_0^- K_{00}^t \,, \tag{97}$$

equations that are clearly of the same form as eqs. (67) and (68), which were obtained in a different way. Coherent coupling between forward- and backward-going waves can only occur (in the first Bragg order) when the propagation constant and the grating constant very nearly satisfy the Bragg condition  $2\beta_0 = K_0 = 2\pi/\Lambda$ . Only those terms on the right-hand sides of eqs. (96) and (97) that are properly phase-matched will be significant; the rest can be neglected, an approximation often termed the synchronous approximation, which leads to

$$\frac{\mathrm{d}A_0^+}{\mathrm{d}z} = \mathrm{i}\kappa A_0^- \,\mathrm{e}^{-\mathrm{i}2\delta z}\,,\tag{98}$$

and

$$\frac{\mathrm{d}A_0^-}{\mathrm{d}z} = -\mathrm{i}\kappa A_0^+ \,\mathrm{e}^{\mathrm{i}2\delta z}\,,\tag{99}$$

where  $\delta$  is a small detuning parameter;  $2\delta = 2\beta_0 - K_0$  ( $\delta = 0$  when the Bragg condition is satisfied exactly). These coupled first-order equations have a relatively simple solution for many problems of interest. It is important to remember, however, that the simple form of eqs. (98) and (99) is based on the approximation in eq. (95). In many cases of practical importance this approximation works quite well. Before turning to the solutions of eqs. (98) and (99), an alternative derivation that is *not* limited to a two-dimensional geometry will be considered for the TE polarization.

# 5.2. IDEAL-MODE EXPANSION – AN ALTERNATIVE APPROACH (TE)

The coupled-mode equations were developed in the previous section by starting with the full mode expansions, eqs. (69) and (70), and then manipulating them in various ways using two of Maxwell's equations. This is in contrast to the method illustrated in eqs. (58) - (68), which showed, for a one-dimensional case, that coupled-mode equations emerge directly from the wave equation. Since only one spatial mode of the waveguide is important for most applications, the full mode expansion is an unnecessary complication. In what follows, the problem of a TE-guided wave propagating in the corrugated structure of fig. 14 will be treated, but the restriction to propagation along z, perpendicular to the grating "rulings" will be lifted. The theoretical development parallels that of eqs. (58)-(68).

Figure 15 illustrates the first-order Bragg interaction considered here. A TE-guided wave propagating in a single-mode planar waveguide at angle  $\theta$  with respect to the z-axis interacts with the periodic structure (having a period  $\Lambda$ ) to produce a backward-going wave. A view of the x-z plane for the corrugated waveguide appears in fig. 14. Once again we assume that the Bragg condition is very nearly satisfied, so that  $\delta$ , defined below eq. (99) with  $\beta_z$  replacing  $\beta_0$ , is small. We seek a solution of the wave equation for the electric field E,

$$\left[\nabla^2 + \frac{\varepsilon(x) + \Delta\varepsilon(x, z)}{\varepsilon_0} k_0^2\right] E(x, y, z, t) = 0, \qquad (100)$$

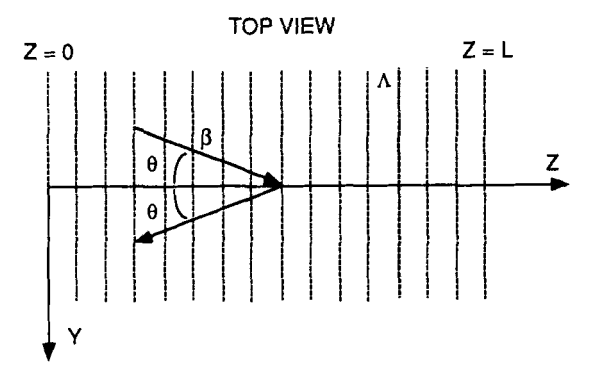


Fig. 15. Top view of a corrugated section of length L of a planar optical waveguide. The grating width along y is taken to be large. A forward-going guided wave with propagation vector  $\beta$ , oriented at angle  $\theta$  with respect to the z-axis, generates a backward-going guided wave by means of the Bragg interaction with the periodic perturbation.

where  $\varepsilon_0$  is the permittivity of free space,  $k_0 = \omega/c = 2\pi/\lambda$ ,  $\varepsilon(x) = n^2(x)\varepsilon_0$  and  $\Delta\varepsilon$  are as defined in eqs. (5) and (91), and the usual time dependence,  $\exp(-i\omega t)$ , is assumed. We adopt the central view of the ideal-mode expansion by considering  $\Delta\varepsilon$  to be a perturbation on the structure of the mean, or ideal, waveguide of refractive index n(x), as shown in fig. 14. The field E is oriented parallel to the y-z plane, and is written in the product form

$$E(x, y, z) = f(z) \exp(i\beta_{\nu} y) E_0^{(i)}(x). \tag{101}$$

The superscript (i) labels the lowest-order ideal mode of the unperturbed, single-mode waveguide [see eq. (6)]. This is equivalent to neglecting the radiation modes in the full mode expansion, acknowledging that the period of the corrugation is such that it provides no coupling between the bound mode and the radiation field.

The ideal mode satisfies the equation

$$\left[\frac{\partial^2}{\partial x^2} + n^2(x)k_0^2\right] E_0^{(i)}(x) = \beta^2 E_0^{(i)}(x). \tag{102}$$

Now, insert eq. (101) into eq. (100), make use of eq. (102), and note that  $\beta = (\beta_v, \beta_z)$  to obtain

$$\left[\frac{\partial^2}{\partial z^2} + \beta_z^2\right] f(z) E_0^{(i)}(x) = -\mu \omega^2 \Delta \varepsilon f(z) E_0^{(i)}(x), \qquad (103)$$

where  $\mu = \mu_0$  = the permeability of free space. The x-dependence can be eliminated from eq. (103) by first multiplying by the complex conjugate of  $E_0(x)^*$  (i.e.  $E_0(x)$ ) integrating over all x, and using the normalization condition in eq. (24), with the result

$$\left[\frac{\partial^2}{\partial z^2} + \beta_z^2\right] f(z) = -2\beta K(z) f(z), \qquad (104)$$

where

$$K(z) = \frac{1}{4}\omega \int_{-\infty}^{\infty} \Delta \varepsilon \, E_0^{(i)}(x) \, E_0^{(i)}(x)^* \, \mathrm{d}x \,, \tag{105}$$

analogous to eq. (85). Equation (104) has the same form as eq. (58), the only difference being that f(z) is now a vector amplitude. This offers no significant complication, however, due to the simple form of the right-hand side of eq. (104).

The same steps that led from eq. (58) to eq. (62), when applied to eq. (104)

give the result

$$f(z) = A^{+}(z) e^{i\beta_z z} + A^{-}(z) e^{-i\beta_z z}, \qquad (106)$$

where  $A^+(z)$  and  $A^-(z)$  are the vector amplitudes of forward- and backward-going (along z) waves. They are given by

$$A^{+}(z) = \frac{\mathrm{i}}{\cos \theta} \int_{-\infty}^{z} \mathrm{e}^{-\mathrm{i}\beta_{z}z'} K(z') f(z') \, \mathrm{d}z' , \qquad (107)$$

and

$$A^{-}(z) = \frac{i}{\cos \theta} \int_{z}^{\infty} e^{i\beta_{z}z'} K(z') f(z') dz'.$$
 (108)

These can be reduced to a pair of coupled, first-order equations by writing the vector amplitudes in terms of unit vectors  $\mathbf{e}_{\pm}$  according to

$$A^{+}(z) = A^{+}(z)e_{\perp}$$
 and  $A^{-}(z) = A^{-}(z)e_{\perp}$ , (109)

where

$$\mathbf{e}_{+} \cdot \mathbf{e}_{+} = 1$$
 and  $\mathbf{e}_{-} \cdot \mathbf{e}_{-} = 1$ . (110)

The unit vectors specify the directions of the electric field vectors for the forward- and backward-going waves. We first form the dot products of eq. (107) and (108) with  $e_+$  and  $e_-$ , respectively, noting that

$$\mathbf{e} \cdot \mathbf{e} = \cos(2\theta)$$
.

to obtain the scalar equations

$$\frac{\mathrm{d}A^{+}}{\mathrm{d}z} = \frac{\mathrm{i}K(z)}{\cos\theta} \left[ A^{+} + A^{-} \cos(2\theta) \,\mathrm{e}^{-\mathrm{i}2\beta_{z}z} \right],\tag{111}$$

and

$$\frac{dA^{-}}{dz} = \frac{-iK(z)}{\cos\theta} \left[ A^{+} \cos(2\theta) e^{i2\theta_{z}z} + A^{-} \right].$$
 (112)

K(z) was evaluated in the previous section [see eq. (92)] for a cosine grating of the type specified in eq. (90):  $K(z) = 2 \kappa \cos(K_0 z)$ , where  $\kappa$  is given by eq. (93). As with eqs. (96) and (97), we retain only the phase-matched terms (synchronous approximation) with the results

$$\frac{\mathrm{d}A^{+}}{\mathrm{d}z} = \mathrm{i}\,\kappa(\theta)A^{-}\,\mathrm{e}^{-\mathrm{i}2\delta z}\,,\tag{113}$$

and

$$\frac{\mathrm{d}A^{-}}{\mathrm{d}z} = -\mathrm{i}\kappa(\theta)A^{+} \,\mathrm{e}^{\mathrm{i}2\delta z}\,,\tag{114}$$

where  $2\delta = 2\beta_z - K_0$ , and

$$\kappa(\theta) = \frac{\kappa \cos(2\theta)}{\cos \theta} \quad \text{(TE-TE)}\,,\tag{115}$$

with  $\kappa$  as given in eq. (93) for TE polarization.

Equations (113) and (114) are in complete agreement with the coupled-mode equations derived earlier using Kogelnik's formalism for  $\theta = 0$ . They are more general, however, in that they apply for arbitrary angle  $\theta$  (see fig. 15). Equation (115) identifies the coupling coefficient  $\kappa(\theta)$  for the TE-TE, first-order Bragg reflection of guided waves. All theoretical treatments of this problem obtain this same result for TE-guided waves for the case of a small surface perturbation  $\Delta h$ .

#### 5.3. SOLUTION OF THE COUPLED-MODE EQUATIONS

The coupled-mode equations in eqs. (113) and (114) can be solved in a straightforward fashion after specifying the appropriate boundary conditions (KOGELNIK [1975]). Here, we consider a surface-corrugation grating of finite length L along the z-axis, but of infinite extent along the y-axis. The upper surface of the perturbed waveguide is, then, given by

$$d = h + \Delta h \cos(K_0 z)$$
  $0 \le z \le L$ ,  
=  $h$  otherwise,

as in fig. 15. The boundary conditions we consider are such that for perfect Bragg matching,  $\delta = 0$ ,

$$A^{+}(z) = 1 \quad z \le 0$$
,  
 $A^{-}(z) = 0 \quad z = L$ . (116)

The conditions at z = 0 and z = L yield the solutions

$$A^{+}(z) = \frac{\alpha \cosh[\alpha(L-z)] - i\delta \sinh[\alpha(L-z)]}{\alpha \cosh(\alpha L) - i\delta \sinh(\alpha L)} \exp(-i\delta z), \qquad (117)$$

and

$$A^{-}(z) = \frac{i\kappa(\theta) \sinh[\alpha(L-z)]}{\alpha \cosh(\alpha L) - i\delta \sinh(\alpha L)} \exp(+i\delta z), \qquad (118)$$

with

$$\alpha = \left\{ \kappa(\theta)^2 - \delta^2 \right\}^{1/2}. \tag{119}$$

We now examine the characteristics of these solutions.

Figures 16 and 17 show plots of  $|A^+(z)|^2$  and  $|A^-(z)|^2$  for  $\kappa(\theta)L = 2$  for perfect Bragg matching ( $\delta = 0$ ) and an illustrative detuning ( $\delta = 1.95/L$ ), respectively. The increased detuning in fig. 17 results in a reduction in the amplitude of the reflected wave at z = 0 to approximately 80% and an accompanying increase in the forward wave amplitude at z = L in comparison with the perfectly Bragg-matched case of fig. 16. The grating reflectivity R is defined as

$$R = \left| \frac{A^{-}(z=0)}{A^{+}(z=0)} \right|^{2}, \tag{120}$$

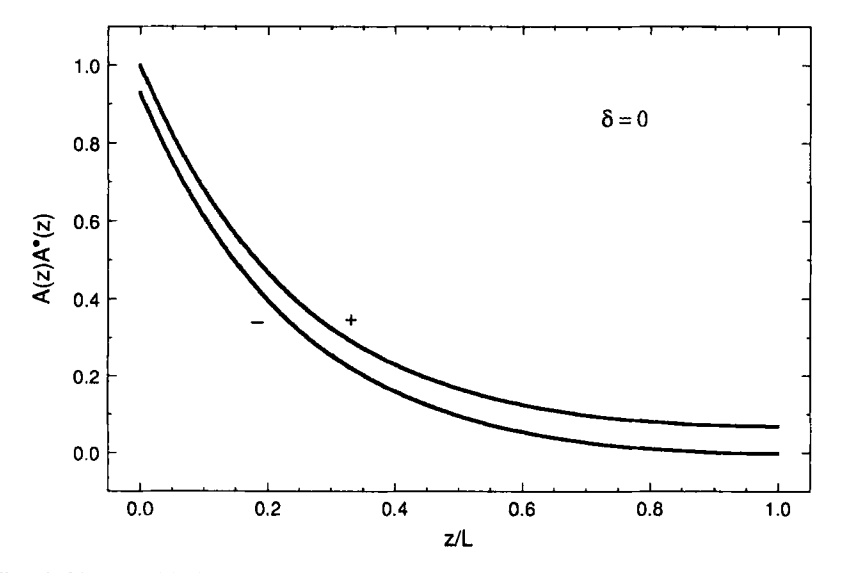


Fig. 16. Plots of  $A(z)A^*(z)$  for forward-going (+) and backward-going (-) waves for  $\kappa(\theta)L=2$  and perfect Bragg matching,  $\delta=0$ .

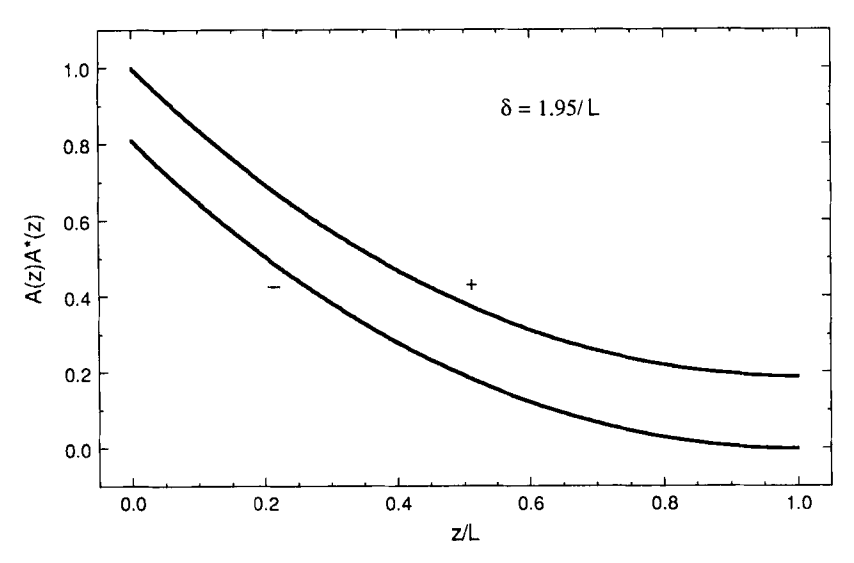


Fig. 17. Plots of  $A(z)A^*(z)$  for forward-going (+) and backward-going (-) waves for  $\kappa(\theta)L = 2$  and sample detuning  $\delta = 1.95/L$ .

so that

$$R = \frac{\sinh^2 \left\{ \kappa(\theta) L \sqrt{1 - \left[ \delta / \kappa(\theta) \right]^2} \right\}}{\cosh^2 \left\{ \kappa(\theta) L \sqrt{1 - \left[ \delta / \kappa(\theta) \right]^2} \right\} - (\delta / \kappa)^2}.$$
 (121)

Note that the form of eq. (121) must be changed to one expressed in terms of sines and cosines for  $\delta/\kappa(\theta) > 1$ .

Figure 18 shows a plot of the reflectivity R versus  $\delta/\kappa(\theta)$  for the two cases  $\kappa(\theta)L=1$  (dashed line) and  $\kappa(\theta)L=2$  (solid line). The larger coupling strength produces the higher peak reflectivity, greater than 90% in this example. Reducing the coupling coefficient  $\kappa(\theta)$  both decreases the maximum reflectivity and broadens the spectral response, as one would expect. The detuning, for a fixed grating period, is a measure of the wavelength (or frequency) deviation from the Bragg-matched value. The Bragg-matched reflectivity R takes on the very simple form

$$R = \tanh^2(\kappa(\theta)L) \quad (\delta = 0), \tag{122}$$

plotted in fig. 19. The reflectivity for  $\delta = 0$  saturates at unity for products of the coupling coefficient and the grating length greater than  $\sim 3$ . The coupling coefficient, of course, depends on the angle of incidence  $\theta$  according to eq. (115)

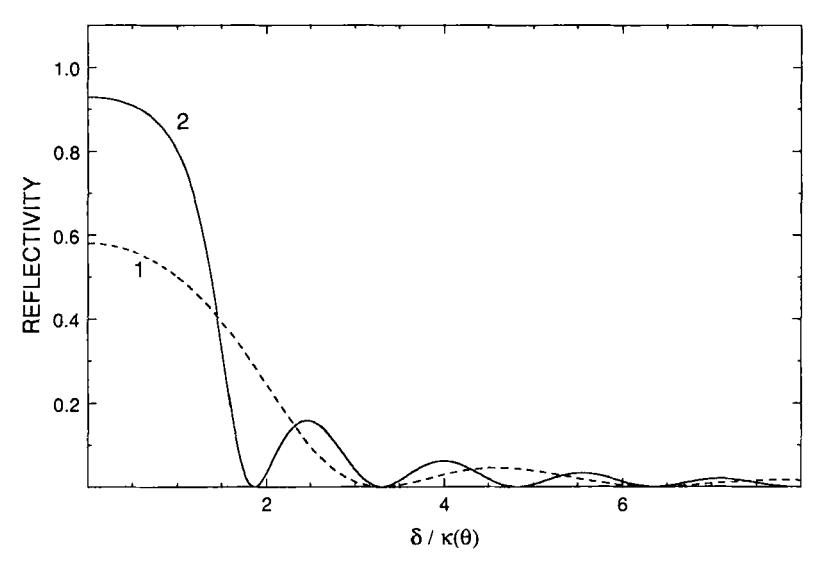


Fig. 18. Plots of the grating reflectivity R, eq. (121), as a function of  $\delta/\kappa(\theta)$  for  $\kappa(\theta)L=1$  (dashed line) and  $\kappa(\theta)L=2$  (solid line).

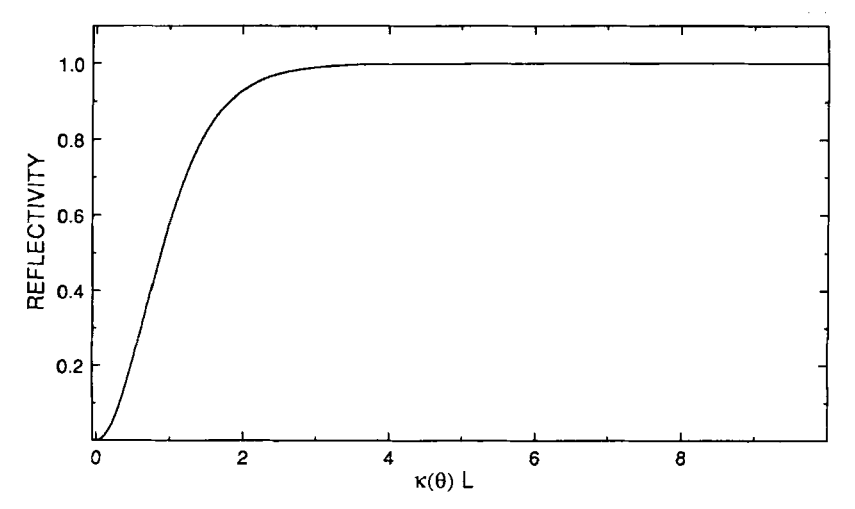


Fig. 19. Grating reflectivity R as a function of the coupling strength  $\kappa(\theta)L$  for the case of pertect Bragg matching,  $\delta = 0$ .

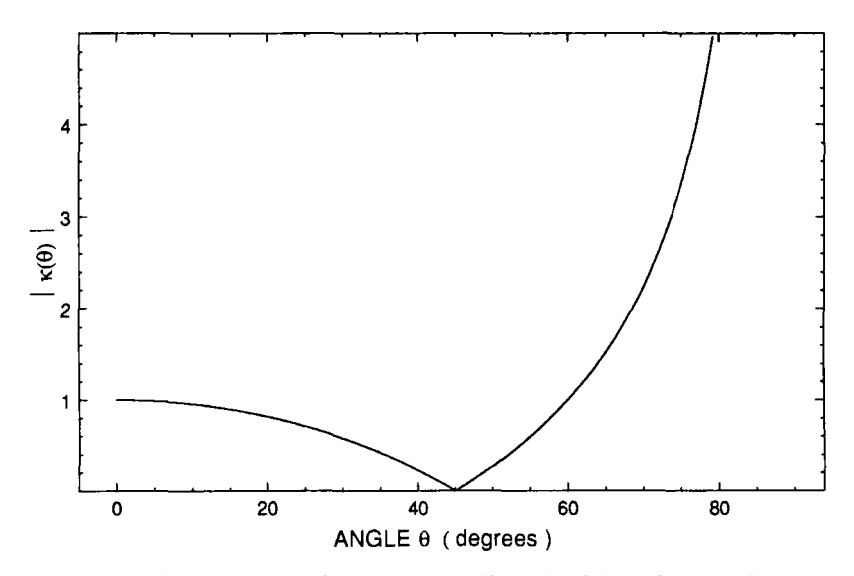


Fig. 20. Normalized absolute value of the coupling coefficient  $|\kappa(\theta)|$  as a function of the angle  $\theta$  (see fig. 15) for TE-polarized incident and diffracted guided waves (TE-TE). Note that  $\kappa(0)$  has been set to unity for simplicity.

for TE-guided waves, a dependence that is illustrated in fig. 20 for the normalization  $\kappa = 1$  at  $\theta = 0$ . The coupling coefficient vanishes at  $\theta = 45^{\circ}$  and rises rapidly as  $\theta \to 90^{\circ}$ . Divergence of the coupling coefficient for  $\theta = 90^{\circ}$  is expected, since this corresponds to grazing incidence for which the reflectivity should approach unity.

#### 5.4. COUPLING BETWEEN TM-GUIDED WAVES

The coupling coefficient  $\kappa(\theta)$  contains the essential information regarding the strength of the interaction between the guided wave and the surface corrugation. As mentioned earlier, the various theoretical approaches generally agree on the matter of the TE-coupling coefficient, eqs. (93) and (115). This was not the case until very recently for the TM-coupling coefficient. It is becoming clear, in fact, that eq. (94), the coupling coefficient obtained from the ideal-mode expansion, is incorrect.

STREIFER, SCIFRES and BURNHAM [1976] were the first to recognize that calculations based on the ideal-mode expansion for TM modes in a waveguide with a corrugated surface led to certain difficulties. They found that various

formulations of the problem led to very different values of  $\kappa$  for the case of a large refractive-index difference at the corrugated boundary. SIPE and STEGEMAN [1979] then reported the results of a comparison (for  $\theta = 0$ ) of the coupling coefficients obtained by the ideal-mode version of coupled-mode theory and by "total field analysis", a theory that attempts to satisfy the boundary conditions at the corrugated surface in an explicit way. They found agreement for the TE case but disagreement for the TM case. STEGEMAN, SARID, BURKE and HALL [1981] generalized the "total field analysis" to arbitrary  $\theta$  and found general disagreement with earlier extensions of the ideal-mode analysis to arbitrary  $\theta$  for the TM case. Gruhlke and Hall [1984] examined (for  $\theta = 0$ ) both the grating-reflection problem and the related problem of the radiation pattern produced by a guided wave interacting with a surface grating. They used a boundary perturbation technique that satisfies the boundary conditions at the corrugated surface to first order in the grating height. Again, the results agreed perfectly with those of the ideal-mode version of coupled-mode theory for TE polarization but disagreed for both problems for the TM polarization.

MARCUSE [1974] describes two different formulations of coupled-mode theory, one of which is based on the *ideal-mode* expansion we have already discussed, and the other based on the so-called *local normal mode* expansion. Whereas the former expands the fields of the corrugated waveguide in terms of the fields of the uncorrugated *mean* waveguide, the latter expands them in terms of the fields for an unperturbed waveguide with the local thickness. The difference between the two is that the location (but not the slope) of the boundary of the perturbed waveguide coincides with that of the unperturbed waveguide for the local normal mode expansion, but not for the ideal-mode expansion. MARCUSE's [1974] analysis for  $\theta = 0$  shows that these two formulations predict different coupling coefficients for the TM polarization.

MARCUSE'S [1974] local normal mode (LNM) analysis was recently generalized to arbitrary angle  $\theta$  by Weller-Brophy and Hall [1988]. The predicted coupling coefficient  $\kappa(\theta)$  (in  $\mu$ m<sup>-1</sup>) appears as the solid curve in fig. 21 for an illustrative choice of parameters ( $n_c = 1.0$ ,  $n_f = 1.56$ ,  $n_s = 1.47$ ,  $h = 0.9 \,\mu$ m,  $\lambda = 0.8 \,\mu$ m). The dashed curve, shown for comparison, is the prediction of the ideal-mode theory of Wagatsuma, Sakaki and Saito [1979]. The LNM analysis is in complete agreement with those theories that satisfy the boundary conditions (to first order in the corrugation height). The most striking feature in fig. 21 is the zero-crossing that occurs near  $\theta = 20^{\circ}$  for the LNM theory, but does not occur for the ideal-mode theory. This suggests that an experiment that examines the grating reflectivity in the vicinity of the

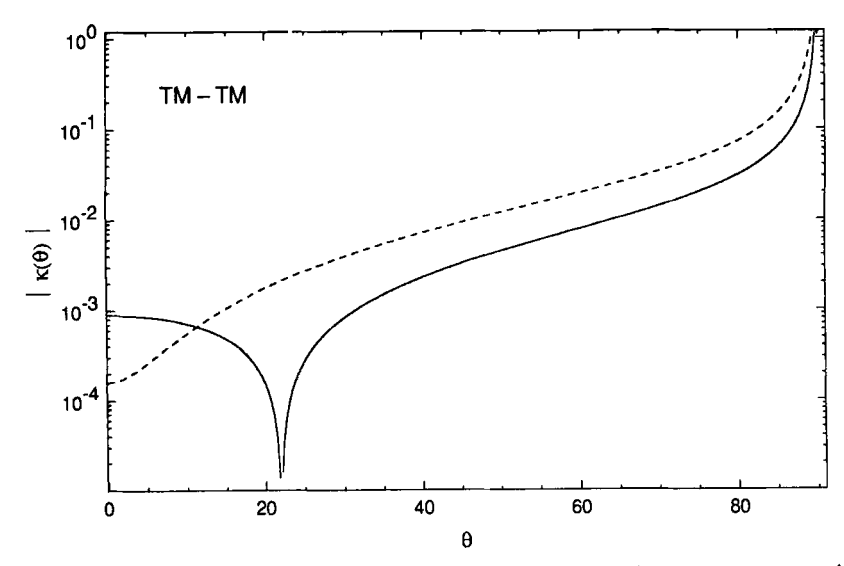


Fig. 21. Angular dependence of the absolute value of the coupling coefficient  $|\kappa(\theta)|$  (in  $\mu$ m<sup>-1</sup>) for TM-polarized incident and diffracted guided waves (TM-TM), as predicted using the local normal mode approximation (solid curve) and the ideal-mode approximation (dashed curve). The parameters used to make the plots are given in the text. The former shows a distinctive zero-crossing that is absent in the latter.

zero-crossing will be a good test of the two theories, since one theory predicts a very small value compared with the other [see eq. (122) for the relation between the reflectivity R and the coupling coefficient  $\kappa(\theta)$ ].

Weller-Brophy and Hall [1987] reported the results of such an experiment. The waveguide and grating parameters were chosen so that, for the experimental conditions, the ideal-mode theory predicted a 100% reflectivity for both the TE and the TM cases, whereas the LNM theory predicted a 100% reflectivity for TE and a 13% reflectivity for TM. The comparison with experiment is summarized in table 1.

Table 1 Comparison of measured and predicted grating reflectivities (in %).

|       | Theory     |                   | Experiment |
|-------|------------|-------------------|------------|
|       | Ideal mode | Local normal mode |            |
| TE-TE | 100        | 100               | 75         |
| TM-TM | 100        | 13                | 9          |

The measured reflectivities agree better with the LNM result. Neither calculation included the effects of propagation losses in the waveguide, so the difference between the measured and calculated LNM values is not considered significant. The large difference between the *measured* TE and TM reflectivities, however, lends strong support to the LNM version of coupled-mode theory as the more correct analysis. It appears, not surprisingly, that the boundary conditions on the corrugated surface must be handled carefully.

# 5.5. LOCAL NORMAL MODE EXPANSION AND COUPLED-MODE EQUATIONS (TM)

The success of the local normal mode (LNM) expansion over the ideal-mode expansion in predicting the results of the measurement described in the previous section for the TM polarization raises the question of the essential difference between the two approaches to the grating reflection problem. Both Marcuse's original derivation for  $\theta = 0$  (Marcuse [1974]) and the extension of this work to arbitrary  $\theta$  (Weller-Brophy and Hall [1988]) are rather cumbersome, however. More importantly, the derivations are sufficiently different so that the connection with that for the ideal-mode approach can be difficult to make. Here, we make use of a new treatment of the LNM approximation that, hopefully, makes the comparison easier. The theoretical development in this section parallels that for the TE polarization presented in eqs. (100)–(115).

We begin with the wave equation in eq. (100), repeated here for convenience,

$$\left[\nabla^2 + \frac{\varepsilon(x) + \Delta\varepsilon(x, z)}{\varepsilon_0} k_0^2\right] E(x, y, z, t) = 0, \qquad (123)$$

and consider the same geometry that appears in fig. 15. As before,  $\Delta \varepsilon$  describes the perturbation [see eq. (91)] introduced into the structure of the mean (or ideal) waveguide, as in fig. 14. Motivated by the earlier treatment of the TE problem, we write the field E in the form

$$E(x, y, z, t) = f(z) e^{i\beta_y y} E_L(x, z) e^{-i\omega t},$$
 (124)

where  $E_L(x, z)$  gives the x-dependence of the electric field profile at a given position z in the perturbed waveguide. In the LNM approximation,  $E_L(x, z)$  is taken to be the field profile for the mode of an uncorrugated waveguide with the local (L) thickness, i.e. that for a given z. As before, we rearrange the wave

equation so that the perturbation term appears on the right

$$\left(\nabla^2 + \frac{\varepsilon(x)}{\varepsilon_0} k_0^2\right) E(x, y, z, t) = -\frac{\Delta \varepsilon(x, z)}{\varepsilon_0} k_0^2 E(x, y, z, t). \tag{125}$$

At this point, eq. (125) still contains the spirit of the ideal-mode expansion, since the permittivity  $\varepsilon(x, z) = \varepsilon(x) + \Delta \varepsilon(x, z)$  has been split into two parts – that for the ideal waveguide  $[\varepsilon(x)]$  and that for the perturbation  $[\Delta\varepsilon(x,z)]$ . The chosen form for the field in eq. (124), however, does not make use of the field profile appropriate for the ideal, uncorrugated waveguide. The essence of the LNM approximation, as treated here, is that the field E is treated differently on the left- and right-hand sides of eq. (125). In particular, the z-dependence in  $E_1(x, z)$  is neglected on the left-hand side, but is retained on the right-hand side. The right-hand side of eq. (125) drives the differential equation, and so great care must be taken to model it as well as possible. This means that the approximate fields in the perturbed regions must be handled carefully. We will return to this point soon. Since it is assumed from the beginning that the perturbation is relatively small, the propagation of the forward- and backwardpropagating waves should not be very different for the corrugated and uncorrugated waveguides. Therefore, we treat  $E_1(x, z)$  on the left as independent of z, and indistinguishable from the field profile for the ideal [superscript (i)] waveguide. With this approximation on the left, eq. (125) becomes

$$E^{(i)}(x) \left[ \frac{\mathrm{d}^2}{\mathrm{d}z^2} + \beta_z^2 \right] f(z) \approx -k_0^2 \left( \frac{\Delta \varepsilon(x, z)}{\varepsilon_0} \right) f(z) E_{\mathrm{L}}(x, z) , \qquad (126)$$

where we have assumed that  $E_L(x, z) \sim E^{(i)}(x)$  satisfies eq. (102), consistent with the approximation.

Next, we integrate the x-dependence out of eq. (126) by first forming the field

$$E_{\beta}^{(i)}(x) = \hat{\mathbf{x}} E_{x}^{(i)}(x) + \left\{ \hat{\mathbf{y}} \left( \frac{\beta_{y}}{\beta} \right) - \hat{\mathbf{z}} (\boldsymbol{\beta} \cdot \hat{\mathbf{z}}/\beta) \right\} E_{z}^{(i)}(x) . \tag{127}$$

The quantities  $E_x^{(i)}(x)$  and  $E_z^{(i)}(x)$  are the components of  $E^{(i)}(x)$  for a forward-going wave propagating along z ( $\beta_y = 0$ ); ^ designates a unit vector. The dot product in eq. (127) is positive (negative) for forward-(backward-) going waves. The amplitude f(z) consists of forward- and backward-going waves, as we have seen earlier in this chapter. The construction in eq. (127) allows us to project the forward-going field onto a backward-going ideal mode, and the backward-going field onto a forward-going ideal mode, to examine their mutual coupling.

We accomplish this by forming the dot product of eq. (126) with the complex conjugate of eq. (127) and then integrating over x, and obtain

$$\left[\frac{\mathrm{d}^2}{\mathrm{d}z^2} + \beta_z^2\right] f(z) = -\left(\frac{4\mu_0\omega}{I_N}\right) K(z) f(z), \qquad (128)$$

where K(z) has the familiar form

$$K(z) = \frac{1}{4}\omega \int_{-\infty}^{\infty} \Delta \varepsilon(x, z) E_{L}(x, z) \cdot \{E_{\beta}^{(i)}(x)\}^* dx, \qquad (129)$$

and  $I_N$  is a normalization integral given by

$$I_{N} = \int_{-\infty}^{\infty} E^{(i)}(x) \cdot \{E_{\beta}^{(i)}(x)\} * dx.$$
 (130)

The normalization integral  $I_N$  is similar to that for TE modes, eq. (24). In fact, the normalization for TM modes given in eq. (25) implies that  $I_N \sim 2\mu_0 \omega/\beta$  for the lowest-order TM mode. (For most cases  $I_N$  rarely differs from  $2\mu_0 \omega/\beta$  by more than 1% for the lowest-order TM mode, primarily because the integral is dominated by the term involving the transverse components of the fields.) Equation (128) becomes

$$\left[\frac{\mathrm{d}^2}{\mathrm{d}z^2} + \beta_z^2\right] f(z) = -2\beta K(z) f(z), \qquad (131)$$

which has the same form as that in eq. (104) for TE modes.

From this point, the analysis proceeds just as before. The Green function technique is used to develop coupled-mode equations, which are then solved using the synchronous approximation [see above eq. (113)]. The all-important coupling coefficient is obtained by writing  $K(z) = 2\kappa \cos(K_0 z)$ , so that

$$\kappa(\theta) = \frac{\kappa'}{\cos \theta},\tag{132}$$

where we recall that the factor  $1/\cos(\theta)$  is contributed by the Green function, since it is proportional to  $1/\beta_z$ .

K(z) must be evaluated carefully.  $E_L(x,z)$  is the model field of an uncorrugated waveguide with the local thickness, whereas  $E^{(i)}(x)$  is described in terms of the modes of the ideal (mean) waveguide. This means that each field must be placed in the correct medium, a point made in the paper by STEGEMAN, SARID, BURKE and HALL [1981]. Table 2 attempts to make the distinction

TABLE 2

Comparison of ideal-mode and local normal mode treatments for the TM-TM interaction (P = perturbed; U = unperturbed).

Coupling integral: 
$$K(z) = \frac{1}{4}\omega \int_{-\infty}^{\infty} \Delta \varepsilon(x, z) E_{\mathbf{P}}(x, z) \cdot \{E_{\mathbf{U}}^{(i)}(x)\}^* dx$$
.

| Ideal mode*                         |  | Local normal mode*   |  |
|-------------------------------------|--|--|--|
|                                     | $\Delta \varepsilon = \varepsilon_0 (n_{\rm f}^2 - n_{\rm c}^2)$   |  |  |
| $\boldsymbol{E}_{\mathrm{Pt}}(x,z)$ | $n = n_c$ , $E_{Pt}(x, z) \approx E_t^{(i)}(h)$                    | $n = n_{\rm f},  \boldsymbol{E}_{\rm Pt}(x,z) \approx \boldsymbol{E}_{\rm t}^{\rm (i)}(h)$ |  |
| $E_{\mathbf{P}z}(x,z)$              | $n = n_c$ , $E_{Pz}(x, z) \approx (n_c/n_f)^2 E_z^{(i)}(h)$        | $n = n_{\rm f},  E_{\rm Pz}(x,z) \approx E_z^{(i)}(h)$                                     |  |
|                                     | $h - \frac{\Delta \varepsilon}{d} = \varepsilon_0 (n_c^2 - n_f^2)$ |  |  |
| $\boldsymbol{E}_{\mathbf{Pt}}(x,z)$ | $n = n_{\rm f},  E_{\rm Pt}(x,z) \approx E_{\rm t}^{\rm (i)}(h)$   | $n = n_c$ , $E_{\rm Pt}(x, z) \approx E_{\rm t}^{(i)}(h)$                                  |  |
| $\boldsymbol{E}_{\mathbf{P}z}(x,z)$ | $n = n_f$ , $E_{Pz}(x, z) \approx (n_f/n_c)^2 E_z^{(i)}(h)$        | $n = n_c$ , $E_{Pz}(x, z) \approx E_z^{(i)}(h)$  |  |

<sup>•</sup> t and z designate the transverse and z-components of the vector fields.

between the ideal-mode and local normal mode approaches clear. For regions d > h, for which the actual surface of the perturbed waveguide extends beyond the mean surface at x = h, the field is approximated by that of a waveguide with constant thickness d using  $n = n_f$ . The same is true for d < h, except that  $n = n_c$ . The correct refractive index is assigned to each perturbation region for the purpose of determining the field. The ratios  $n_c/n_f$  and  $n_f/n_c$  that appear in the expressions for the z-components of the fields in table 2 for the ideal mode case are the result of assigning a refractive index other than the actual one to each perturbation region. When evaluated properly, eq. (132) becomes

$$\kappa(\theta) = \frac{\frac{\pi}{\lambda} \frac{\Delta h}{h_{\text{eff}}} \frac{n_{\text{f}}^2 - N^2}{N} \frac{1}{q_{\text{c}}} \left[ \frac{N^2}{n_{\text{f}}^2} - \left( \frac{N^2}{n_{\text{c}}^2} - 1 \right) \cos(2\theta) \right]}{\cos \theta}$$
 (TM - TM),

for the cosine surface grating of eq. (90). Note that  $q_c$  was defined in eq. (32), and all quantities should be evaluated for the lowest-order TM mode. Equation (133) is in complete agreement with that obtained by Weller-Brophy and Hall [1988], and is also in agreement with that obtained by Stegeman, Sarid, Burke and Hall [1981] after a few minor algebraic corrections are made. A comparison with Kogelnik's result, eq. (94), for  $\theta = 0$  shows agreement, provided the quantity in curly brackets in eq. (94) is set to unity, as mentioned earlier. Indeed, it is eq. (133) that is plotted in fig. 21 (solid line) and has so far shown good agreement with experimental results (Weller-Brophy and Hall [1987]). Equation (115) is obtained when the method discussed in this section is applied to the TE-TE Bragg reflection problem; thus, the method is both straightforward and reliable.

The ideal mode approach to the grating reflection problem differs from the treatment given in this section in two ways. First, the LNM approach does not weight the z-component of E differently from the transverse components of E, as is the case for the ideal-mode approximation. This follows as a natural consequence of the assumption that  $E_L(x, z)$  is evaluated as the mode of an ideal waveguide with the local thickness. Second, the net effect of treating  $E_L(x, z)$  this way is that products of the field components in eq. (129) contain one field for each medium, the cover and the film, a feature not present in the ideal-mode approach. The success of the various versions of the LNM approximation highlights the importance of treating the field very carefully in the perturbation term in the wave equation.

#### 5.6. SUMMARY OF COUPLED-MODE TREATMENTS

The previous sections reveal several important points about coupled-mode formulations. First, derivations of the coupled-mode equations, eq. (113) and (114), often make use of a slowly varying envelope approximation, in which the second derivatives of both the forward- and backward-wave amplitudes with respect to z are neglected. This is a completely unnecessary approximation. Both the Green function approach and other formulations arrive at the proper equations without invoking such an approximation. Second, some researchers have asserted that the case of non-normal incidence to the grating "rulings" cannot be treated by solving the wave equation directly (Popov and Mashev [1985a,b]). They argue that one must begin the analysis at a low level, so to speak, with Maxwell's curl equations. The Green function method discussed here demonstrates that this statement is incorrect. Third, the flaw in the

reasoning behind the ideal-mode expansion treatment of the grating-reflection problem was revealed to be an improper treatment of the fields in the region of the surface corrugation. The wave equation contains a perturbation term proportional to  $(\Delta \varepsilon) E$ , in which E must be considered to be a field in the actual medium for the perturbed structure, one for which the permitivity is  $\varepsilon(x) + \Delta \varepsilon(x, z)$ . The ideal-mode expansion violates this to produce two errors, an improper treatment of the z-component of the field [see eq. (84)] and an improper evaluation of the field within each perturbation region in the coupling coefficient. The LNM expansion suffers from neither of these difficulties, since the boundary for the local normal mode  $E_{\rm I}(x,z)$  occurs at the same location as, but with different slope than, that for the actual waveguide field. Previous derivations of the LNM results (MARCUSE [1974], WELLER-BROPHY and HALL [1988]) obtain the correct coupled-mode equations and coupling coefficients for both the TE-TE and TM-TM cases, but the Green function technique obtains the same results for the lowest-order (m = 0) modes with much less labor and in a more direct manner from the wave equation.

#### 5.7. PERTURBATIVE TREATMENT

The previous treatments of the problem of guided waves interacting with a surface-corrugation grating have considered the coupling per unit length between the incident and Bragg-reflected waves to be weak. This is implied in the restriction that the ratio  $\Delta h/h$  or  $\Delta h/\lambda$  is small, which allows the coupling coefficient  $\kappa(\theta)$  to be expressed in a relatively compact form. These same treatments, however, allow the total interaction to be large so that the depletion of the incident wave cannot be neglected. The weak coupling between the forward- and backward-going waves that occurs within any single period of the corrugated waveguide can build up coherently when the Bragg condition is at least nearly satisfied. In this way, even a weak interaction can produce a nearly 100% conversion between the two waves in a finite, but sufficiently long, structure. Thus we see that the coupling coefficient describes the interaction per unit length, whereas the coupled amplitude equations describe the relative amplitudes of the forward- and backward-going waves.

A few authors have attempted to reduce the complexity of the waveguide grating problem by separating the two main parts of the problem (STEGEMAN, SARID, BURKE and HALL [1981]). First, the coupling coefficient is determined in the weak-scattering limit in which one ignores the depletion of the incident wave. The coupling coefficient is subsequently inserted into a pair of coupled-

mode equations to obtain the full solution including depletion. This approach offers the advantage that  $\kappa(\theta)$  can be determined, in principle, to arbitrary precision by using a power-series expansion in, e.g.,  $\Delta h/h$ . It has the disadvantage, however, that the coupled-mode equations must be obtained separately, a process that has led to errors in the past when these equations have been obtained rather intuitively (STEGEMAN, SARID, BURKE and HALL [1981]). The technique for obtaining the coupling coefficient for one such perturbation approach is illustrated in this section.

Tuan [1973], Tuan and Ou [1973], and Tsai and Tuan [1974] used a surface-perturbation theory formulated by CHEN [1968] to examine the scattering of guided waves by a single groove or deformation in the surface of an otherwise unperturbed planar optical waveguide. The technique is based on an expansion of the scattered field and the boundary conditions in power series in the parameter  $\Delta h/h$ , which is presumed to be small. Their theoretical work does not treat the grating problem explicitly, although it also applies to that case. This discussion will assume that the surface-corrugation waveguide grating in fig. 14 is the structure of ultimate interest. HALL [1980] has shown that for the problem of a guided wave that radiates due to the interaction with a surface structure, the first-order (in  $\Delta h/h$ ) boundary perturbation method leads to the same result as the coupled-mode theory of MARCUSE [1974] for the TE polarization, but to different results for the TM polarization (GRUHLKE and HALL [1984]). Again, the disagreement for the TM case is due to the same shortcoming on the part of the ideal-mode expansion, discussed in the previous section. The boundary-perturbation method gives the correct result.

The boundary-perturbation theory was originally formulated in two dimensions, but was later extended to three dimensions (HALL [1981]). Since this section merely aims to outline the methodology, the simpler two-dimensional case will be considered; i.e., we will examine the Bragg reflection of a guided wave incident on a grating at normal incidence ( $\theta = 0$  in fig. 15). The grating length L is taken to be sufficiently small so that depletion of the incident wave can be neglected. The more difficult TM-TM case will be considered here to make a strong connection with the content of the previous section, although the theory also works well for the TE polarization. The basic geometry is shown in fig. 9.

The upper surface x = d of the waveguide is taken to be of the form

$$d = h\{1 + \eta \rho(z)\} \quad \text{for } 0 < z < L \,, \tag{134}$$

and uncorrugated with d = h, otherwise. The parameter  $\eta$  is small, and  $\rho(z)$  describes the surface perturbation. The magnetic field for the TM polarization

is oriented along the y-direction,

$$H = \hat{\mathbf{y}} H_{\nu} \,. \tag{135}$$

The field  $H_{\nu}$  is expanded as the sum of two parts,

$$H_{\nu} = H_{\nu, \text{ inc}} + H_{\nu, \text{ scatt}}. \tag{136}$$

The incident fields, labeled "inc", are taken to be those given in eq. (10), the fields for the unperturbed waveguide of thickness h, for a forward-going wave according to

$$H_{y, \text{inc}} = H_m(x) \exp\left[i(\beta z - \omega t)\right]. \tag{137}$$

The scattered field in medium j is expanded in a power series in the small parameter  $\eta$ ,

$$H_{\text{scatt}}^{(j)} = \sum_{n=1}^{\infty} \eta^n H_{\text{s}n}^{(j)}, \tag{138}$$

where  $H_{sn}$  is the *n*th-order scattered field, and j = s, f, or c in the substrate, film, or cover regions, respectively. For a surface grating of the form of interest here,  $\rho(z) = \cos(K_0 z)$  and  $\eta = \Delta h/h$ .

The boundary conditions on the tangential components of E and H can both be expressed in terms of H by using the unit normal  $u_n$  to the corrugated surface. Both  $H_y$  and  $(1/\varepsilon)u_n \cdot \nabla H_y$  must be continuous across the corrugated interface between the cover and film media. This is difficult to accomplish exactly, but the boundary conditions can be expanded in a power series in  $\eta$  and satisfied up to a specified order in  $\eta$ . The operator  $u_n \cdot \nabla$  can be written in terms of the surface profile as

$$\mathbf{u}_{n} \cdot \nabla = \left\{ 1 + \left( \eta h \, \frac{\mathrm{d}\rho(z)}{\mathrm{d}z} \right)^{2} \right\}^{-1/2} \left\{ \frac{\partial}{\partial x} - \eta h \, \frac{\mathrm{d}\rho(z)}{\mathrm{d}z} \, \frac{\partial}{\partial z} \right\}. \tag{139}$$

When the boundary conditions are satisfied through first order in  $\eta$ , we obtain

$$H_{s1}^{(c)}(h,z) - H_{s1}^{(f)}(h,z) = h\rho(z) \left[ \frac{\partial}{\partial x} \left\{ H_{\nu,\,\text{inc}}^{(f)}(x,z) - H_{\nu,\,\text{inc}}^{(c)}(x,z) \right\} \right]_{x=h}^{\infty} \equiv M_1(z),$$
(140)

and

$$\left[\frac{1}{n_c^2} \frac{\partial H_{s1}^{(c)}(x,z)}{\partial x} - \frac{1}{n_f^2} \frac{\partial H_{s1}^{(f)}(x,z)}{\partial x}\right]_{x=h} \equiv M_2(z), \qquad (141)$$

where

$$M_{2}(z) = h\rho(z) \left[ \frac{1}{n_{f}^{2}} \frac{\partial^{2} H_{y, \text{inc}}^{(f)}(x, z)}{\partial x^{2}} - \frac{1}{n_{c}^{2}} \frac{\partial^{2} H_{y, \text{inc}}^{(c)}(x, z)}{\partial x^{2}} \right]_{x = h}$$

$$+ h \frac{d\rho(z)}{dz} \left[ \frac{1}{n_{c}^{2}} \frac{\partial H_{y, \text{inc}}^{(c)}(x, z)}{\partial z} - \frac{1}{n_{f}^{2}} \frac{\partial H_{y, \text{inc}}^{(f)}(x, z)}{\partial z} \right]_{x = h}. \quad (142)$$

As before, the superscripts (c) and (f) on the incident fields designate the medium in which eq. (137) will be evaluated. The bottom surface of the waveguide at x = 0 is taken to be uncorrugated, of course, so that the first-order boundary conditions produce the much simpler requirements

$$H_{s,1}^{(f)}(0,z) = H_{s,1}^{(s)}(0,z), \tag{143}$$

and

$$\frac{1}{n_{\rm f}^2} \left. \frac{\partial H_{\rm s\,I}^{\rm (f)}(x,z)}{\partial x} \right|_{x=0} = \frac{1}{n_{\rm s}^2} \left. \frac{\partial H_{\rm s\,I}^{\rm (s)}(x,z)}{\partial x} \right|_{x=0}. \tag{144}$$

Equations (140)–(144) can be solved for the unknown first-order scattered fields by introducing plane-wave expansions for  $H_{\rm s\,I}$  in all three media. We write

$$H_{s1}^{(c)}(x,z) = \frac{1}{2\pi} \int_{-\infty}^{\infty} U(\xi) e^{i\xi z} e^{i\xi_c x} d\xi, \qquad (145)$$

$$H_{s1}^{(f)}(x,z) = \frac{1}{2\pi} \int_{-\infty}^{\infty} \left[ V_1(\xi) e^{i\xi_f x} + V_2(\xi) e^{-i\xi_f x} \right] e^{i\xi z} d\xi, \qquad (146)$$

$$H_{s1}^{(s)}(x,z) = \frac{1}{2\pi} \int_{-\infty}^{\infty} W(\xi) e^{i\xi z} e^{-i\xi_s x} d\xi, \qquad (147)$$

where

$$\xi_{j} = \left\{ n_{j}^{2} \left( \frac{\omega}{c} \right)^{2} - \xi^{2} \right\}^{1/2} \quad (j = c, f, s).$$
 (148)

These reduce eqs. (140)–(144) to a set of algebraic equations that can be solved for the amplitudes U,  $V_1$ ,  $V_2$ , and W.

The procedure is rather tedious, but the integral expressions for the fields are versatile. The radiation fields can be determined very easily in the far-field by applying the method of steepest descents. The field for the reflected field in the

waveguide can be obtained by noting that the integrals contain simple poles at  $\xi = \pm \beta$ . The pole at  $\xi = -\beta$  gives the field for the "backscattered" guided wave. Again, the process is rather tedious, but the result is quite simple. For example, the first-order scattered field within the waveguide layer is obtained from eqs. (138) and (146) to be

$$H_{\text{scatt}}^{(f)} \approx i \left[ \left( \frac{\pi}{\lambda} \frac{\Delta h}{h_{\text{eff}}} \frac{n_{\text{f}}^2 - N^2}{N} \frac{1}{q_{\text{c}}} \right) \left( \frac{N^2}{n_{\text{f}}^2} - \frac{N^2}{n_{\text{c}}^2} + 1 \right) \right] L H_m(x) e^{-i(\beta z - \omega t)},$$
(149)

where  $H_m(x)$  refers to the field in the film region 0 < x < h [see eq. (10)]. A comparison with eq. (133) reveals that the quantity in square brackets is just the coupling coefficient  $\kappa(\theta)$  evaluated for  $\theta = 0$ , as required by the two-dimensional geometry (implied normal incidence) considered here. The field is, then, just

$$H_{\text{scatt}}^{(f)} \approx i \kappa(0) L H_m(x) e^{-i(\beta z - wt)}. \tag{150}$$

This means that the back-reflected wave has the same spatial profile as the incident wave, and has strength proportional to  $\kappa(\theta)L$ .  $\kappa(0)$  can, therefore, be interpreted as the fraction per unit length of the incident field coupled from the forward-going incident wave into the backward-going reflected wave, consistent with the interpretation earlier in the chapter.

The agreement between  $\kappa(0)$  in eq. (150) and eq. (133) is illuminating. The former was obtained by satisfying the boundary conditions to first order in the presumed small parameter  $\Delta h/h$ . The latter was obtained from coupled-mode theory, which typically makes no explicit use of the boundary conditions. The afore-mentioned agreement gives some confidence that eq. (133) can be relied upon, provided  $\Delta h/h$  is small.

## 5.8. TE-TM MODE CONVERSION

The previous sections focused on the issue of a correct formulation of the TE-TE and TM-TM Bragg interactions in a corrugated optical waveguide. These are not the only possibilities, however, since for non-normal incidence TE-TM mode conversion also occurs in an optical waveguide. That is, for incident angle  $\theta_i \neq 0$ , a TE- or TM-guided wave incident on a corrugated section of an optical waveguide can, in first order, generate a TM- or TE-

reflected guided wave if the Bragg condition

$$\left(\frac{2\pi N_{\rm TE}}{\lambda}\right)\cos\left(\theta_{\rm i}\right) + \left(\frac{2\pi N_{\rm TM}}{\lambda}\right)\cos\left(\theta_{\rm r}\right) = \frac{2\pi}{\Lambda},\tag{151}$$

is at least nearly satisfied. In this case the incident and reflected guided waves will propagate at the different angles  $\theta_i$  and  $\theta_r$  with respect to the grating normal, since the effective index of refraction  $(N_{\rm TE})$  for the TE polarization differs from that  $(N_{\rm TM})$  for the TM polarization in a given waveguide, even though both are of the same vacuum wavelength  $\lambda$ . The local normal mode approximation also can be used to give a satisfactory result for this case (Weller-Brophy and Hall [1988]). Only the result for the coupling coefficient is given here (note the dependence on two angles),

$$\kappa(\theta_{\rm i}, \theta_{\rm r}) = i\sqrt{C_{\rm TE}} \sqrt{C_{\rm TM}} \frac{(N_{\rm TM}^2 - n_{\rm c}^2)^{1/2}}{q_{\rm c}^{1/2} n_{\rm c}} \frac{\sin(\theta_{\rm i} + \theta_{\rm r})}{\cos(\theta_{\rm r})}$$
 (TE-TM), (152)

where we have used the notation of Weller-Brophy and Hall [1988] so that

$$C_m = \frac{\pi}{\lambda} \frac{\Delta h}{h_{\text{eff. m}}} \frac{n_{\text{f}}^2 - N_{\text{m}}^2}{N_{\text{m}}} \quad (m = \text{TE, TM}).$$
 (153)

There is no TE-TM mode conversion for normal incidence  $\theta_i = \theta_r = 0$ .

## § 6. Summary

This chapter has considered the interaction between the modes of a planar optical waveguide and a periodic surface corrugation, which is an important interaction in many applications. The specific case of the grating-induced coupling between two guided waves in a planar waveguide structure received the principal emphasis here, since it has been the subject of some controversy over the last ten years, a controversy that has only recently been resolved. The physical nature of the interaction is well understood, namely, as being due to Bragg scattering. The quantitative details are complicated, however, by the mode structure characteristic of even an elementary planar optical waveguide. Approximations that work very well and lead to excellent agreement with each other for TE-polarized guided waves disagree with each other significantly for TM-polarized guided waves. A recent experiment was able to distinguish between classes of theories. Those theories based on the familiar ideal-mode

expansion discussed in several textbooks and monographs disagree with the measured results for the TM polarization. Those theories based on either the local normal mode expansion or boundary perturbation techniques agree well with each other and with the experiments. The local normal mode theory makes no explicit consideration of the boundary conditions at the corrugated interface. The boundary perturbation techniques, in contrast, satisfy the boundary conditions up to a desired order in the grating height. It is interesting that two such different approaches should agree so well.

After examining the fundamental principles of importance for a variety of optical waveguides, discussion turned to the various techniques used to attack the problem of a guided wave interacting with a waveguide diffraction grating. An attempt was made to formulate the various approaches to enable a comparison among the various treatments. It emerged that the deficiency in theories based on the ideal-mode expansion can be attributed to an improper treatment of the electric field in the perturbation regions. In essence, these theories ascribe the wrong polarization (in the dipole sense) to the perturbation regions by consistently embedding the approximate fields in the wrong media. A new, very direct formulation of the local normal mode approximation avoided the complexities of earlier versions of the theory and make it relatively easy to identify the principal features of the approximation that make it so successful. We now appear to have at our disposal a theoretical description of the guided-wave Bragg-reflection problem that can be relied upon, at least for the case of shallow surface corrugations. Equally importantly, our understanding of the way in which the problem must be treated has improved. This will likely be of benefit in future treatments of scattering problems in optical waveguides, particularly those that involve TM-polarized guided waves.

# List of Symbols

| a              | asymmetry parameter               |
|----------------|-----------------------------------|
| $A^+(z)$       | forward-wave amplitude            |
| $A^{-}(z)$     | backward-wave amplitude           |
| c              | speed of light in vacuum          |
| D              | power parameter                   |
| E              | electric field                    |
| $E_m(x)$       | electric field profile            |
| $E_{mi}(x)$    | transverse component of $E_m(x)$  |
| $E_m^{(i)}(x)$ | field profile for ideal waveguide |

| $E_{\rm L}(x,z)$                | local normal mode                      |
|---------------------------------|--|
| $E_{\rm c}$                     | $E_m(x)$ at $x = h$                    |
| $E_{\rm s}$                     | $E_m(x)$ at $x = 0$                    |
| $\vec{E_{\mathrm{f}}}$          | maximum value of $E_m(x)$              |
| e <sub>+</sub> , e <sub>-</sub> | unit vectors                           |
| G(x)                            | nonlinear field profile                |
| g(z,z')                         | Green function                         |
| h ,                             | waveguide thickness                    |
| $h_{ m eff}$                    | effective waveguide thickness          |
| H                               | magnetic field                         |
| $H_m(x)$                        | magnetic field profile                 |
| $H_{ml}(x)$                     | transverse component of $H_m(x)$       |
| $H_{\rm c}$                     | $H_m(x)$ at $x = h$                    |
| $H_{\rm s}$                     | $H_m(x)$ at $x=0$                      |
| $H_{ m f}^{'}$                  | maximum value of $H_m(x)$              |
| $H_m^{(i)}(x)$                  | field profile for ideal waveguide      |
| $I_N$                           | normalization integral                 |
| $K(z), K_{mn}(z)$               | coupling integral                      |
| $K_{mn}^{t}, K_{mn}^{z}$        | transverse- and z-parts of $K_{mn}(z)$ |
| $K_0$                           | grating constant $(2\pi/\Lambda)$      |
| $k_{\rm f}$                     | field profile parameter                |
| L                               | length of corrugated region            |
| m                               | mode integer or polarization index     |
| N                               | effective index of refraction          |
| $n_{\rm s}$                     | substrate refractive index             |
| $n_{\rm c}$                     | cover refractive index                 |
| $n_{\mathrm{f}}$                | film refractive index                  |
| n(x)                            | x-dependent refractive index           |
| $n_2$                           | nonlinear coefficient                  |
| $N_{\mathrm{TE}}$               | TE mode effective index                |
| $N_{TM}$                        | TM mode effective index                |
| $q_{\rm c}, q_{\rm s}$          | TM mode parameters                     |
| R                               | reflectivity                           |
| S                               | time-averaged Poynting vector          |
| $\boldsymbol{u}_{\mathrm{n}}$   | unit surface normal                    |
| V                               | nonlinear waveguide parameter          |
| В                               | propagation constant                   |
| $\gamma_c$ , $\gamma_s$         | field decay constants                  |
| 107 13                          | •                                      |

| δ  | detuning parameter          |
|--|-----------------------------|
| Δ  | index offset parameter      |
| Δε   | permittivity perturbation   |
| $\Delta h$                                 | surface grating amplitude   |
| $\varepsilon(x)$                           | x-dependent permittivity    |
| $\boldsymbol{\varepsilon}_0$               | permittivity of free space  |
| η  | surface height parameter    |
| $\theta$                                   | propagation angle           |
| ^  | designates unit vector      |
| κ  | coupling coefficient        |
| λ  | wavelength in vacuum        |
| Λ  | grating period              |
| $\mu_0$                                    | permeability of free space  |
| $\rho(z)$                                  | surface profile             |
| $\phi_{\rm c},\phi_{\rm s}$                | TIR half-phase shifts (TE)  |
| $\phi_{\rm c}^{ m tm},\phi_{ m s}^{ m tm}$ | TIR half-phase shifts (TM)  |
| ω  | (angular) optical frequency |
|  |                             |

### References

ADAMS, M. J., 1981, An Introduction to Optical Waveguides (Wiley, New York).

CHEN, Y. M., 1968, J. Math. Phys. 9, 439.

CONWELL, E. M., 1973, Appl. Phys. Lett. 23, 328.

DAKSS, M. L., L. KUHN, P. F. HEIDRICH and B. A. SCOTT, 1970, Appl. Phys. Lett. 16, 523.

DALGOUTTE, D. C., 1973, Opt. Commun. 8, 124.

EVANS, G. A., J. M. HAMMER, N. W. CARLSON, F. R. ELIA, E. A. JAMES and J. B. KIRK, 1986, Appl. Phys. Lett. 49, 314.

FLANDERS, D. C., H. KOGELNIK, R. V. SCHMIDT and C. V. SHANK, 1974, Appl. Phys. Lett. 24, 194.

FUKUZAWA, T., and M. NAKAMURA, 1979, Opt. Lett. 4, 343.

GRUHLKE, R. W., and D. G. HALL, 1984, Appl. Opt. 23, 127.

GRUSS, A., K. T. TAM and T. TAMIR, 1980, Appl. Phys. Lett. 36, 523.

HALL, D. G., 1980, Appl. Opt. 19, 1732.

HALL, D. G., 1981, Opt. Lett. 6, 601.

Hall, D. G., 1987, in: Integrated Optical Circuits and Components, ed. L. D. Hutcheson (Dekker, New York).

HANDA, Y., T. SUHARA, H. NISHIHARA and J. KOYAMA, 1980, Opt. Lett. 5, 309.

HATAKOSHI, G., and S. TANAKA, 1978, Opt. Lett. 2, 142.

HOCKER, G. B., and W. K. BURNS, 1975, IEEE J. Quantum Electron. QE-11, 270.

KOGELNIK, H., and C. V. SHANK, 1971, Appl. Phys. Lett. 18, 152.

KOGELNIK, H., and C. V. SHANK, 1972, J. Appl. Phys. 43, 2327.

KOGELNIK, H. G., 1975, in: Applied Physics, Integrated Optics, Vol. 7, ed. T. Tamir (Springer, New York).

KOGELNIK, H. G., 1988, in: Electronics and Photonics, Guided-Wave Optoelectronics, Vol. 26, ed. T. Tamir (Springer, New York).

KOROTKY, S. K., and R. C. ALFERNESS, 1987, in: Integrated Optical Circuits and Components, ed. L. D. Hutcheson (Dekker, New York).

KURMER, J. P., and C. L. TANG, 1983, Appl. Phys. Lett. 42, 146.

LIN, Z., S. ZHOU, W. S. C. CHANG, S. FOUOUHAR and J. M. DELAVAUX, 1981, IEEE Trans. Microwave Theory and Tech. MTT-29, 881.

LIVANOS, A. C., A. KATZIR, A. YARIV and C. S. HONG, 1977, Appl. Phys. Lett. 30, 519.

MACOMBER, S. H., J. S. MOTT, R. J. NOLL, G. M. GALLATIN, E. J. GRATRIX, S. L. O'DWYER and S. A. LAMBERT, 1987, Appl. Phys. Lett. 51, 472.

MARCUSE, D., 1974, Theory of Dielectric Optical Waveguides (Academic Press, New York). MILLER, S. E., 1969, Bell Syst. Techn. J. 48(7), 2059.

NAKAMURA, M., A. YARIV, H. W. YEN, S. SOMEKH and H. L. GARVIN, 1973, Appl. Phys. Lett. 22, 515.

PENNINGTON, K. S., and L. KUHN, 1971, Opt. Commun. 3, 357.

POPOV, E., and L. MASHEV, 1985a, Opt. Acta 32, 265.

POPOV, E., and L. MASHEV, 1985b, Opt. Acta 32, 635.

SHELLAN, J. B., C. S. HONG and A. YARIV, 1977, Opt. Commun. 23, 298.

SIPE, J. E., and G. I. STEGEMAN, 1979, J. Opt. Soc. Am. 69, 1676.

SOMEKH, S., and A. YARIV, 1972, Opt. Commun. 6, 301.

STEGEMAN, G. I., D. SARID, J. J. BURKE and D. G. HALL, 1981, J. Opt. Soc. Am. 71, 1497.

STEGEMAN, G. I., J. J. BURKE and C. T. SEATON, 1987, in: Integrated Optical Circuits and Components, ed. L. D. Hutcheson (Dekker, New York) and references therein.

STONE, F. T., and S. AUSTIN, 1976, IEEE J. Quantum Electron. QE-12, 727.

STREIFER, W., D. R. SCIFRES and R. D. BURNHAM, 1975, IEEE J. Quantum Electron. QE-11, 867.

STREIFER, W., D. R. SCIFRES and R. D. BURNHAM, 1976, IEEE J. Quantum Electron. QE-12, 74.

SUHARA, T., and H. NISHIHARA, 1986, IEEE J. Quantum Electron. QE-22, 845.

TSAI, T. L., and H. S. TUAN, 1974, IEEE J. Quantum Electron. QE-10, 326.

TUAN, H. S., 1973, IEEE Trans. Antennas & Propag AP-21, 351.

TUAN, H. S., and C. H. Ou, 1973, J. Appl. Phys. 44, 5522.

WAGATSUMA, K., H. SAKAKI and S. SAITO, 1979, IEEE J. Quantum Electron. QE-15, 632.

WELLER-BROPHY, L. A., and D. G. HALL, 1987, Opt. Lett. 12, 756.

WELLER-BROPHY, L. A., and D. G. HALL, 1988, J. Lightwave Tech. LT-6, 1069.

YAMAMOTO, Y., T. KAMIYA and H. YANAI, 1978, IEEE J. Quantum Electron. QE-14, 245.

YARIV, A., 1973, IEEE J. Quantum Electron. QE-9, 919.

YI-YAN, A., C. D. WILKINSON and P. J. R. LAYBOURN, 1980, IEEE J. Quantum Electron. QE-16, 1089.